Spring 2023

Nonlinear Dynamics Analysis and Control of Space Vehicles with Flexible Structures

Marco Fagetti
Embry-Riddle Aeronautical University, fagettim@my.erau.edu

By

A Thesis Submitted to the Faculty of Embry-Riddle Aeronautical University

In Partial Fulfillment of the Requirements for the Degree of

Master of Science in Aerospace Engineering

Embry-Riddle Aeronautical University

Daytona Beach, Florida

By

THESIS COMMITTEE

Graduate Program Coordinator, Dr. Hever Moncayo	Date
Dean of the College of Engineering, Dr. James W. Gregory	Date
Associate Provost of Academic Support, Dr. Christopher Grant	Date

ACKNOWLEDGMENTS

First and foremost, I would like to thank my family for their endless guidance, encouragement, support, and love throughout my life and educational career. Without them, my interests and passion for Astronautics and Aerospace Engineering would have never blossomed as they have, and this achievement would not have been possible.

I would also like to thank my advisor, Dr. Morad Nazari, for his invaluable guidance and patience throughout my higher education. He has been a wonderful role model who saw my potential to perform great advancements in the field of Aerospace Engineering. His compassion for his students' happiness and well-being is as vast as the knowledge and experience that he passionately and readily imparts whenever I am in need of advice and direction. This research effort would not have been possible without him.

There are also several committee and non-committee members I would like to thank. Thank you for all of the time, ideas, guidance, motivation, and knowledge that assisted in the progression and towards the completion of my research and higher education. Finally, thank you to all of my fellow colleagues that I have met and come to consider my friends. Your friendships, stories, support, and companionship have brought endless laughter, comfort, and inspiration during my time as a university student.

ABSTRACT

Space vehicles that implement hardware such as antennas, solar panels, and other extended appendages necessary for their respective missions must consider the nonlinear rotational and vibrational dynamics of these flexible structures. Formulation and analysis of these flexible structures must account for the rigid-flexible coupling present in the system dynamics for stability analysis and control design. The system model is represented by a flexible appendage attached to a central rigid body, where the flexible appendage is modeled as a cantilevered Euler-Bernoulli beam. Discretization techniques, such as the assumed modes method and the finite element method, are used to model the coupled dynamics by transforming the partial differential equations of motion into a finite set of differential equations. State feedback control laws are designed to achieve stability and desired motion in the presence of rigid-flexible coupling. An optimal controller in the form of a linear quadratic regulator (LQR) is presented and compared with a Lyapunov-based control law that guarantees asymptotic stability. Conventional and adaptive sliding mode control (SMC) laws are also presented to account for any uncertainties in the linearized system model. Full-order (FO) and reduced-order (RO) observers are included in the control system to account for lack of velocity state measurements that are generally unavailable in real world applications. The results demonstrated that the Lyapunov-based and LQR control laws both control the motion of the rigid-flexible system and suppress flexible vibrations. Appropriate tuning of the control gains and weighting matrices, respectively, determines the settling time and overshoot of the system response as well as vibration suppression during motion. The results also demonstrated that the SMCs are capable of correcting for any uncertainties in the system model. Conventional SMCs (CSMC) required a longer convergence time, and chattering was significant for one CSMC. The adaptive sliding mode control provided quick convergence to the ideal trajectory while also avoiding chattering. Lastly, the FO and RO observers provided quick estimation of the states that were implemented in the control laws.

TABLE OF CONTENTS

LIST OF FIGURES

Figure **Page**

LIST OF TABLES

Table **Page**

1 Introduction

This chapter introduces the idea of coupled body dynamics of space vehicles with flexible structures and its interaction with control systems. The nonlinear dynamics of a rigid-flexible structure can be discretized into a linear set of differential equations that provide an accurate approximation of the rigid-flexible dynamics that can be implemented in closed-loop feedback control design. Firstly, previous research and analytical history of the dynamics of flexible structures, particularly those attached to space vehicles, and the control laws designed and implemented for such systems are presented. Next, the motivation and objective of this thesis research are stated, followed by the organization of this thesis.

1.1 Background and Literature Review

The physical phenomenon of structural-flexibility present in structural dynamics and its effects on control design and application is not unique to spacecraft design and control. In fact, it has caused considerable difficulty as a persistent challenge throughout engineering history in the development and practical application of aircraft, missiles, and launch vehicles [2]. Lack of knowledge on the interaction between flexible structures, their rigid-body counterparts, and the designed vehicle control systems can lead to unforeseen consequences, ranging from small, stable oscillations to motions and interactions of such magnitude that may lead to system instability and possible mission failure. The first satellite launched into space by the United States and successfully achieve orbit, Explorer I, was designed in such a way that it was considered to be sufficiently rigid so that, in the presence of low magnitude forces and moments from the space environment, any rigid-flexible coupling interactions with the control systems could be considered negligible. However, the presence of the four flexible whip antennae invalidated the necessary complete rigid body assumption that ensures spin-stabilization about the principle moment of inertia. Soon after orbital insertion, the intended motion was unstable and the spin axis was diverging from the minimum inertia axis [3, 4]. Experiences and post-flight analyses of other space vehicles and missions over time, such as Ranger, Alouette I and II, the 1963-22A satellite, and the OGO-III (Orbit-

ing Geophysical Observatory) satellite, have provided valuable insight on the effects that the nonlinear dynamic behavior of flexible structures have on the resulting vehicle motion, stability, and control system outcomes as well as effective methods of accounting for this coupled interaction [3, 4].

Structural flexibility of a space vehicle with flexible components is intrinsic in the vehicles dynamics. The translational and rotational dynamics of a rigid-body spacecraft under numerous different conditions and environments have been analytically derived and numerically simulated with relative ease. However, the presence of a flexible structure or appendage, such as a communication antennae or solar panel, immediately necessitates major changes in the formulation of the systems equations of motion [5]. Unfortunately, the nonlinear ordinary and partial differential equations of motion of a space vehicle with flexible structures require a different analytical approach from the traditional methods of analysis. The common approach initially applied, and still utilized today, for the vibration analysis of elastic systems consists of formulating continuous, differentiable systems of second-order differential equations through a specified method. Initially, the normal-coordinate method traditionally used in vibration analysis was considered. This approach formulates the equations of motion as a system of independent and uncoupled scalar second-order differential equations. The use of modal coordinates and the independence of these normal-mode coordinates permits the independent calculation of their participation in the vehicle motion. This is the key feature of the normal-coordinate approach because it permits the exercise of engineering judgment in determining which coordinates are so significant as to warrant retention, and which may be abandoned in coordinate truncation [5]. However, this method has not been widely used due to its theoretical and practical limitations and underlying assumptions. Instead, methods of analysis that involve series discretization of the system have gained more traction and appreciation for their generality, especially with the help of technological advancements in computer hardware and software. The chosen method is often applied in conjunction with the Newton-Euler equations [6–10] or the Hamiltonian or Lagrangian approach [11].

The origin of the series discretization methods can be traced to Rayleigh's energy method, a technique for approximating the lowest natural frequency of a conservative system [12–14]. It is based on Rayleigh's principle, which states that Rayleigh's quotient has a minimum value equal to the lowest eigenvalue when the trial function used in conjunction with Rayleigh's quotient is the lowest eigenfunction. To improve the approximation, it is only necessary to find a trial function capable of lowering the approximation. This is the essence of the Rayleigh-Ritz method [12]. Several other methods have built upon the fundamental principal of the Rayleigh-Ritz method: lumped-parameter method, truncated mode method, method of weighted residuals, the Galerikin method, etc. Furthermore, numerous research papers, journals, and projects have utilized these different methods to discretize these nonlinear equations of motion of rigid-flexible structures [15–19]. A technique known as the assumed modes method (ASM) is regarded by some as the Rayleigh-Ritz method. It is more physically motivated, and it obtains the same results as the Rayleigh-Ritz method. Another technique that is similar to the Rayleigh-Rits method but has only been in existence since the 1950s is the finite element method (FEM) [20]. This method found use early on as a solution for structural-related problems involving geometrically complicated and irregular structures. However, the versatility of this method resulted in an explosion of interest across many scientific fields. FEM works similarly to the ASM, utilizing trial, or admissible, functions. What distinguishes the two is that FEM employs local functions defined over small subdomains instead of global functions over the entire system domain. This concept curried favor for FEM because it permitted small, good approximations to be realized with local admissible functions in the form of low-degree polynomials instead of requiring lengthy derivations of complex global admissible functions that can only be applied to a select few problems.

Finally, consideration of nonlinear rigid-flexible coupling in the dynamics of a space vehicle plays a critical role in the design and implementation of closed-loop control systems. Exclusion of the flexibility effect from the mathematical model of the system can lead to not

only errors in control effort requirements and positioning inaccuracies but also instabilities. The vibrations of the attached flexible structures excited by external forces or spacecraft control inputs can induce small to severe reaction torques and forces at a large range of frequencies on the space vehicle. Control systems for rigid-flexible space vehicles require very accurate mathematical models in order to account for and reduce this vibration as much as possible [21]. Generally, only the displacement of flexible structures can be measured with sensors, such as strain gauges and piezoelectric sensors [22]. Another challenge in control design is the lack of full-state measurements of the flexible structure. Unless full knowledge of the system's states is assumed, some form of state estimator or observer-based control is necessary for closed-loop feedback control. Many studies have been conducted with a large variety of both nonlinear and linear controllers with and without state observers [23–27]. Because different control laws provide distinct benefits, a variety of approaches have been considered. Robust control allows for compensation against disturbances and uncertainties in the system but often require knowledge of the system model. Meanwhile, adaptive control laws are better suited for optimizing cycle time and control effort without necessarily knowing the dynamics of the system [28]. Several adaptive approaches for the control of a rigid-flexible structure with model uncertainties include an adaptive active control by Gaudiller and Bochard [29] that makes it possible to render nearly constant the dynamic behavior of multi-articulated flexible structures in spite of changes in the geometry of their masses and an adaptive control by Balas and Frost [30] that uses residual mode filters to compensate for troublesome modal subsystems that may inhibit the requirements of Almost Strict Positive Realness when the system has unknown modeling parameters and poorly known operating conditions .

1.2 Research Motivation and Objective

To the author's knowledge, most research that analyzes the dynamics and control design for space vehicles with flexible structures consider only the nonlinear equations of motion or utilize more traditional linearization and discretization methods. Not as much research that

formulates the dynamics of rigid-flexible structures with FEM and utilizes those systems of equations to design feedback control laws has been conducted. Furthermore, most works mention the presence of rigid-flexible coupling in the nonlinear dynamics of rigid-flexible systems and its effects; however, they often do not expand on the topic and provide an analytical representation of the coupling. This research formulates the dynamics of the system by applying two discretization techniques that provide an analytical set of system equations containing the dynamic behavior of the rigid body, the flexible structure, and the rigid-flexible interaction between the two. Closed-loop feedback control systems are designed in this thesis with the formulated dynamics in mind such that the rigid-flexible system is controlled by a single control torque input applied to the central rigid body of the system. The objective of the control laws is to propagate the system from an initial state to a desired state while minimizing the vibrations of the flexible structure and counteracting the rigid-flexible coupling present when the system is in motion. In order to account for a system with uncertainties in the model, robust control laws are also implemented in the control systems. An ASMC developed by Cho et al. [31] is compared with CSMCs. However, this thesis expands the utility of the ASMC to include vector-matrix variables and provides an adapted stability analysis.

1.3 Thesis Organization

The content of this thesis following the introduction of the dynamics analysis and control design of rigid-flexible space vehicles begins with Chapter 2, where the preliminary mathematical model that describes the elastic behavior of an Euler-Bernoulli beam is presented, along with the system model for a rigid-body space vehicle with a flexible appendage that will be adopted for this thesis. A space vehicle with flexible structures requires a mathematical model that can accurately characterize the behavior of the flexible body. The characteristic design and behavior of an Euler-Bernoulli beam provides an accurate initial model of a flexible structure. The full rigid-body system model and its nonlinear ordinary and partial differential equations of motion are presented at the end of Chapter 2, along with

the boundary conditions accompanied with the specified model.

The formulation of the rigid-flexible system dynamics through the application of two discretization methods is presented in Chapter 3. This chapter explains the theoretical concept of ASM and FEM, followed by the complete derivation of the space vehicle's linearized equations of motion through both methods. Since the formulation of dynamics from these two methods does not include damping in the system, the introduction and incorporation of proportional damping into the system is presented. At the end of Chapter 3, an analytical comparison of ASM and FEM is presented, from which the dynamics formulated from FEM are selected to be used in the control design and numerical simulations presented later on in the thesis. Chapter 4 presents the stability analysis and control laws designed for closed-loop feedback control of the rigid-flexible system. The equations of motion developed from Chapter 3 are rewritten in a state-space representation, and the stability of the system is studied through the application of Lyapunov's direct and indirect methods. Before designing any control law, the system's observability and controllability are studied to ensure control law requirements are satisfied. Full-state feedback control laws are first discussed. Besides the Lyapunov-based control law defined through the stability analysis of the system, optimal control and robust control are considered. The general linear quadratic regulator (LQR) that minimizes a quadratic cost function to regulate the system's states to zero is presented for optimal control. Sliding mode control (SMC) that utilizes a sliding manifold to control the system trajectory is presented for robust control. The conventional SMC (CSMC) that utilizes a linear sliding manifold is discussed and implemented with different mathematical functions that have varying degrees of effect on the control effort produced by the CSMC. An adaptive SMC (ASMC) developed by Cho et al. [31] that utilizes a nonlinear sliding manifold and an adaptive law that tunes the SMC in in real-time is also presented. These SMCs serve to account for any uncertainties present in the mathematical model of the rigid-flexible system. Chapter 4 ends with a derivation for a full-order (FO) and reduced-order (RO) observer for observer-base control design.

Numerical simulations and discussions for the rigid-flexible system under open-loop and closed-loop feedback control are given in Chapter 5. To analyze the dynamic effects of a flexible structure on a rigid-body spacecraft, an open-loop simulation of the system without control law is performed. The interaction between the control system and rigid-flexible coupling is also analyzed through a comparison of the different state-feedback control laws applied to both an ideal system and a system with uncertainties. The impact and effectiveness of observer-based feedback control on the system is also analyzed. Lastly, conclusions and ideas for future work are provided in Chapter 6.

2 Mathematical Modeling of the System

A model of a space vehicle with flexible structures is required to analyze the dynamics design control laws for the rigid-flexible structure. The model specified must consist of structures that replicate the dynamic behavior of both a rigid body and flexible structure.

2.1 Euler-Bernoulli Beam

For the flexible structure attached to the rigid body space vehicle, an Euler-Bernoulli beam is considered as the flexible model. As such, the flexible model is modeled as a long, slender structural member subjected to transverse loading that produces significant bending effects as opposed to twisting or axial effects. This bending deformation is measured as a transverse displacement and a rotation. Hence, the degrees of freedom considered per node along the beam are a transverse displacement and a rotation [1]. Generally, beams have a small cross-sectional area relative to their lengths. The calculations for the load-carrying and deflection characteristics of an Euler-Bernoulli beam can be simplified without too much loss of accuracy.

It is important to note that, as mentioned before, twisting and axial effects are not considered as significant as the bending effects. For an Euler-Bernoulli beam, several further assumptions about the beam are made. The shape and geometry of the beam's cross-sections do not change significantly. During deformation, the cross-section of the beam remains planar and normal to the deformed neutral axis of the beam. Lastly, the deformed beam angles, or slopes, remain small despite the neutral axis becoming curved. Therefore, as per the use of an Euler-Bernoulli beam, shear deformation and axial deformation are not considered.

Before creating the full rigid-flexible dynamical model, the model and sign conventions of the beam are established. Consider the beam element shown in Figure 2.1. The beam is of length l with axial local coordinate x and transverse local coordinate y. The local transverse nodal displacements are denoted by $\hat{d}_{i_y}$'s and the rotations by $\hat{\phi}_i$'s. The local nodal forces are denoted by $\hat{f}_{i_y}$'s and the bending moments by $\hat{\tau}_i$'s as shown. The distributed load along the length of the beam is denoted by $w(x)$. Once again, all axial effects are neglected. At

all nodes, the following sign conventions are used:

1. Displacements and forces are positive in the positive y direction.

2. Rotations and moments are positive in the counter-clockwise direction.

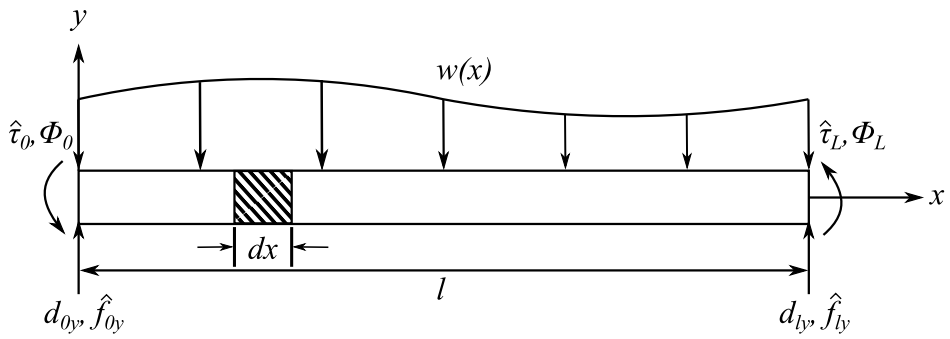

Figure 2.1 Beam element displaying positive nodal displacement, rotation, force, and moment direction and subjected to applied loads [1].

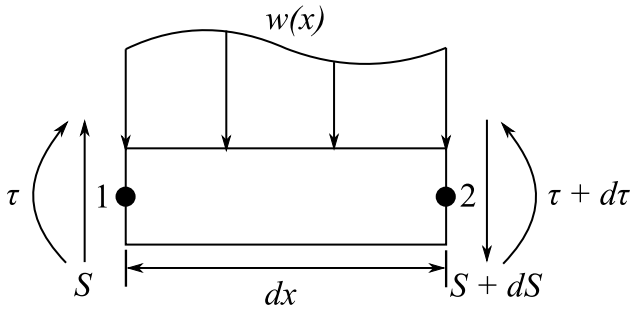

Figure 2.2 Differential beam element.

Formulation of a beam's characteristic behavior requires the elementary linear-elastic beam differential equation to be first developed. The differential equation governing elementary linear-elastic beam behavior [32] (called the Euler-Bernoulli beam as derived by Euler and Bernoulli) is based on plane cross sections perpendicular to the longitudinal centroidal axis of the beam before bending occurs remaining plane and perpendicular to the longitudinal axis after bending occurs. This occurs in practice only when a pure couple or constant moment exists in the beam. However it is a reasonable assumption that yields equations that quite accurately predict beam behavior for most practical beams [1].

Consider the Euler-Bernoulli beam element in Figure 2.1 subjected to applied loads $\hat{f}_{0_y}$ and $\hat{f}_{l_y}$ and a distributed load $w(x)$ that cause deformations along the length l of the beam element. From force and moment equilibrium of a differential element of the beam, shown in Figure 2.2, we have

$$\sum F_y = 0 : S - (S + dS) - w(x)dx = 0 \tag{2.1}$$

$$\sum \tau_2 = 0 : -Sdx + d\tau + w(x)dx\left(\frac{dx}{2}\right) = 0 \tag{2.2}$$

Simplifying Eqs. (2.1) and (2.2) yields

$$w(x) = -\frac{dS}{dx} \tag{2.3}$$

and

$$S(x) = \frac{d\tau}{dx} \tag{2.4}$$

The final form of the shear force in Eq. (2.4) that relates the shear force to the bending moment is obtained by dividing Eq. (2.2) by dx and taking the limit of the equation as dx approaches 0. The $w(x)$ term disappears when Eq. (2.3) is substituted into Eq. (2.2), becoming negligibly small. The curvature of the beam and its relation to moment is

$$\kappa = \frac{1}{r} = \frac{\tau}{EI} \tag{2.5a}$$

where r is the radius of the deflected curve of the beam after some displacement occurred, E is the modulus of elasticity of the beam, and I is the area moment inertia of the beam.

For small slopes, where the rotational displacement at a node along the beam is $\phi = \frac{dy}{dx}$, the curvature is given by

$$\kappa = \frac{d^2y}{dx^2} \tag{2.5b}$$

where y is the transverse displacement function. Applying Eq. (2.5b) in Eq. (2.5a), the equation for moment is obtained as

$$\tau(x) = EI\frac{d^2y}{dx^2} \tag{2.6}$$

Substituting τ from Eq. (2.6) into Eq. (2.4) gives the equation for shear force:

$$S(x) = EI\frac{d^3y}{dx^3} \tag{2.7}$$

Substitution of S in Eq. (2.3) produces the beam differential equation

$$\frac{d^2}{dx^2}\left(EI\frac{d^2y}{dx^2}\right) = -w(x) \tag{2.8a}$$

Assuming there is no distributed load along the beam, i.e $w(x) \equiv 0$, and the EI is constant, the final differential beam equation is reduced to

$$EI\frac{d^4y}{dx^4} = 0 \tag{2.8b}$$

2.2 2-D Rigid-Flexible System Model

The system model is comprised of two components: a rigid-body central hub and a flexible-body appendage, or structure. Both parts are assumed to have constant uniform

masses and moments of inertia. The rigid-body central hub is modelled as a circular rigid-body with a body-fixed frame fixed at the origin of the inertial reference frame. The flexible structure is modelled as an Euler-Bernoulli beam with uniform mass density and the preceding assumptions stated in the previous section. The flexible structure is considered cantilevered to the central rigid body at one end and free at the other end. The rigid-flexible system is also controlled by a scalar control torque applied to the central rigid body. The system is assumed to move only in a planar rotational motion. This is an important assumption of the system model that follows into the formulation of the system dynamics. Figure 2.3 provides a visual representation of the 2-D rigid-flexible system model.

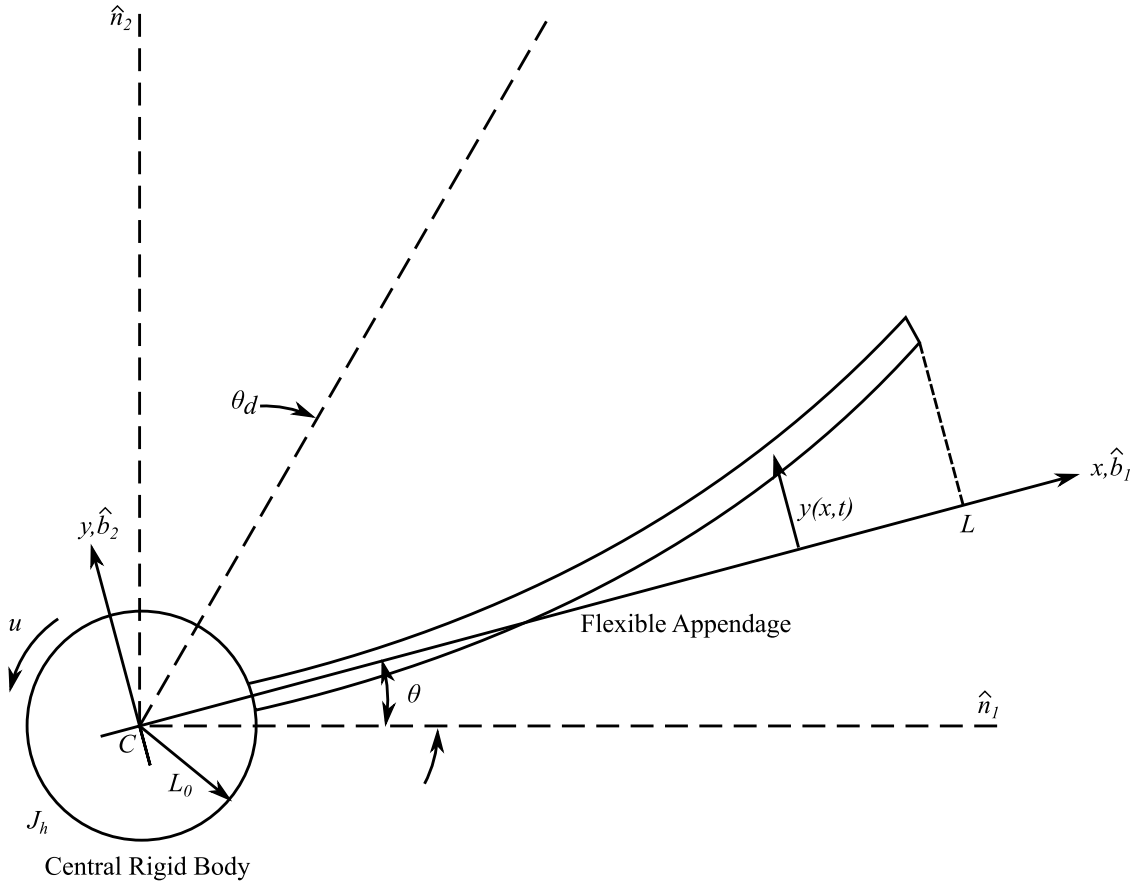

Figure 2.3 Rigid-flexible body system model.

The central rigid body has a moment of inertia J_h and a radius denoted as L_0. The control torque input applied to the central rigid body is denoted a u and is a function time.

The flexible structure has a total length L. The inertial reference frame $\mathcal{N} : \{\mathcal{C}, \widehat{n}_1, \widehat{n}_2, \widehat{n}_3\}$ shares its origin $\mathcal{C}$ with the body-fixed frame $\mathcal{B} : \left\{\mathcal{C}, \widehat{b}_1, \widehat{b}_2, \widehat{b}_3\right\}$, where $(\widehat{\ })$ denotes a unit vector. The rotation of the central rigid body is denoted by θ with a final desired angular position θ_f. The flexible structure's transverse displacement is a function of time t and position x and denoted by $y(x,t)$ in the $\widehat{b}_2$ axis, where x is the position coordinate along the $\widehat{b}_1$ axis.

The hybrid system of ordinary and partial differential equations governing the dynamics of this system is readily obtained from Hamilton's principle to be [33, 34]

$$J_h \frac{\partial^2 \theta}{\partial t^2} = u + (\tau_0 - S_0 L_0) \tag{2.9a}$$

$$-(\tau_0 - S_0 L_0) = \int_0^L \rho x \left(\frac{\partial^2 y}{\partial t^2} + x \frac{\partial^2 \theta}{\partial t^2} \right) \mathrm{d}x + \text{H.O.T.} \tag{2.9b}$$

$$\rho \left(\frac{\partial^2 y}{\partial t^2} + x \frac{\partial^2 \theta}{\partial t^2} \right) + EI \frac{\delta^4 y}{\delta x^4} = 0 + \text{H.O.T.} \tag{2.9c}$$

The boundary conditions that accompany a cantilevered Euler-Bernoulli beam that is pinned at one end, i.e. $x = 0$, and free at the other end, i.e. $x = L$, are [1, 14, 33, 34]:

$$y|_{(x=0)} = \frac{\partial y}{\partial x}\Big|_{(x=0)} = EI \frac{\partial^2 y}{\partial x^2}\Big|_{(x=L)} = EI \frac{\partial^3 y}{\partial x^3}\Big|_{(x=L)} = 0 \tag{2.10}$$

In the following chapter, two discretization techniques are introduced to formulate a linearized system of equations. The discretized displacement along the length of the flexible structure is substituted into the mathematical model characterized by Eqs. (2.9a), (2.9b), and (2.9c). These equations are also utilized in the derivation of the Lyapunov-based control law in Chapter 4.

3 Dynamics Approximation Using Assumed Modes and Finite Element Methods

The formulation of the dynamics of a rigid-flexible system can be accomplished through several methods, such as the lumped-parameter method, Myklestad's method, the Rayleigh-Ritz method, the method of weighted residuals, the Galerkin method, etc. [12, 14]. This chapter covers and utilizes two of those methods – assumed modes method and finite element method – and explains the motivation behind which is used for the continuation of the work. Both of these approaches lead to linear, finite-dimensional, continuous-time equations of motion for approximating the dynamics of rigid-flexible structures.

3.1 Assumed Modes Method

The assumed modes method is a procedure for the discretization of distributed systems closely related to the Rayleigh-Ritz method [35]. Although the motivation and details are different, the results are the same as those obtained by the Rayleigh-Ritz method using the energy form of Rayleigh's quotient. The main advantage of the assumed modes method is that it is somewhat easier to grasp. However, this method may require significant problem-solving through trial-and-error if the interest lies in the finer points of analysis [14].

In the assumed modes method, the deflection of continuous elastic structures is modeled by a finite series of space-dependent functions that are multiplied by specified time-dependent amplitude functions [13, 36–39]. The amplitudes become a set (or subset) of generalized configuration coordinates, in the usual Lagrangian interpretation of generalized coordinates. The space-dependent functions are typically chosen as a complete set of linearly independent functions, selected to satisfy at least the geometric boundary conditions, and they differentiate at least half as many times as the order of the system. All such functions are referred to as admissible functions.

Admissible functions are the most widely encountered choice for the basis functions in the assumed modes method. However, if the problem formulation and a priori insight permit, the basis functions may be selected to satisfy, in addition, some or all of the physical (nat-

ural) boundary conditions, and are differentiable as many times as the order of the system. This more restricted subset of admissible functions that satisfy both geometric and physical boundary conditions are referred to as comparison functions. With comparison functions, more efficient convergence can be obtained as a general rule, but cannot be guaranteed for every forced response application. That is, for a given number of functions, we expect better accuracy in approximating the true system dynamics when using comparison functions instead of admissible functions [33].

While the best space-dependent functions are usually the system's eigenfunctions, which satisfy not only all boundary conditions but also the rigorous spatial differential equations (resulting from the separation of variable technique applied to the governing partial differential equations), these are not always available. This is because the rigorous partial differential equations must usually be formulated and solved exactly to obtain the eigenfunctions and, obviously, it is impossible to carry these developments to completion for complicated structures. It is difficult to converge exactly on all of the eigenvalues and the corresponding eigenfunctions, even when an analytically derived characteristic equation can be obtained, because the number of eigenfunctions which can be retained is finite, and the arithmetic errors made in solving the characteristic equation to obtain the eigenvalues cannot always be ignored [33]. The assumed modes approach is shown to be useful for problems whose geometry is sufficiently simple to permit the insight necessary to select a "good" set of global displacement functions [14].

In order to derive the equations of motion, consider the rigid-flexible system in Figure 2.3, modeled in Chapter 2. Note that L_0 is the radius of the rigid hub, x is the coordinate of a mass element measured along the undeformed beam, and $y(x,t)$ is the local deformation measured perpendicular to the x axis. The inertial position vector $\bar{r}(x,t)$ that goes from the origin to a deformed point in the flexible structure is given by

$$\bar{r}(x,t) = (L_0 + x)\hat{b}_1 + y\hat{b}_2 \tag{3.1}$$

where ($\hat{}$) denotes a unit vector. The velocity of the deformed point is then

$$\dot{r}(x,t) = \frac{d}{dt}(r) + \omega \times r = -\dot{\theta} y \widehat{b}_1 + (\dot{y} + \dot{\theta}(L_0 + x))\widehat{b}_2 \tag{3.2}$$

where $\omega = \dot{\theta}\widehat{n}_3 = \dot{\theta}\widehat{b}_3$ is the angular velocity of the central rigid body in both the inertial and body-fixed frames. To enforce zero elongation, small radial motion along $\widehat{b}_1$ is neglected. This yields the final velocity

$$\dot{r}(x,t) = (\dot{y} + \dot{\theta}(L_0 + x))\widehat{b}_2 \tag{3.3}$$

In order to apply the Lagrangian approach, the kinetic and potential energies of the rigid-flexible system are obtained. The total kinetic energy is expressed as the sum of the rigid body's kinetic energy and flexible structure's kinetic energy, i.e.,

$$T = T_{hub} + T_{app} = \frac{1}{2} J_h \dot{\theta}^2 + \int_0^L \rho \dot{\bar{r}} \cdot \dot{\bar{r}} \, \mathrm{d}x \tag{3.4}$$

where J_h is the rotary inertia of the rigid body, $\dot{\theta}$ is the angular velocity of the rigid body, L is the length of the appendage, and ρ is the linear mass density of the flexible structure. Substituting the velocity in Eq. (3.3) into Eq. (3.4) leads to a quadratic expression of the kinetic energy as a function of the spatial integrals in the form

$$T \frac{1}{2} \hat{J} \dot{\theta}^2 + \int_0^L \rho \dot{y}^2 \, \mathrm{d}x + \dot{\theta} \int_0^L \rho (L_0 + x) \dot{y} \, \mathrm{d}x \tag{3.5}$$

where the total moment of inertia $\hat{J}$ is

$$\hat{J} = J_h + 2 \int_0^L \rho (L_0 + x)^2 \, \mathrm{d}x \tag{3.6}$$

The total potential energy of the rigid-flexible system under the Euler-Bernoulli assumptions is expressed as

$$V = \int_0^L EI(y'')^2 \, \mathrm{d}x \tag{3.7}$$

where EI is the flexural rigidy of the flexible structure, and $(\cdot)''$ denotes the second partial derivative of $(\cdot)$ with respect to x.

To generate an $\mathcal{A}$ degree-of-freedom approximate differential equation model for a continuous system, the displacement of the continuous system is expanded as a linear combination of $\mathcal{A}$ prescribed shape functions. Thus the deformation $y(x,t)$ is approximated by

$$y(x,t) = \sum_{j=1}^{\mathcal{A}} \psi_j(x) q_j(t), \quad j = 1, \cdots, \mathcal{A}, \quad 0 \leq x < L \tag{3.8}$$

where $\psi_j(x)$ denotes jth assumed mode shape, $q_j(t)$ denotes the jth generalized coordinate, and $\mathcal{A}$ denotes the number of terms retained in the approximation. The approximate expansion Eq. (3.8) will be used in conjunction with Lagrange's equations to obtain a finite-dimensional approximate system of ordinary differential equations of motion that govern the time evolution of the amplitudes $q_j(t)$.

The admissible functions derived by [33]

$$\psi_j(x) = 1 - \cos\left(\frac{j\pi x}{L}\right) + \frac{1}{2}(-1)^{j+1}\left(\frac{j\pi x}{L}\right)^2, \quad \text{for } j = 1, \cdots, \mathcal{A} \tag{3.9}$$

satisfy the geometric and physical boundary conditions of a clamped-free beam, and have been found to be excellent admissible functions for clamped free appendages [33]. Through substitution of Eqs. (3.8) and (3.9) into Eqs. (3.5) and (3.7), the finitie dimensional systm of ordinary differential equations of motion for $\theta(t)$, and $q_j(t)$ can be derived by using the Lagrangian approach, i.e.,

$$\frac{d}{dt}\left(\frac{\delta T}{\delta \dot{\tilde{q}}_j}\right) - \left(\frac{\delta T}{\delta \tilde{q}_j}\right) + \left(\frac{\delta V}{\delta \tilde{q}_j}\right) = F \tag{3.10}$$

where F is the generalized force, and $\tilde{q}_j$ is the jth element of the configuration vector $\tilde{q}$, i.e.,

$$\tilde{q} = [\theta, q_1, q_2, \ldots, q_{\mathcal{A}}]^T \tag{3.11}$$

The generalized force F can be determined by finding the virtual work, δW, associated with the control torque, u. For a general motion of the system, the total work done by the control torque is

$$W = \int_{x_1}^{x_2} u \, \mathrm{d}\theta \tag{3.12}$$

where x_1 and x_2 denote arbitrary initial and final configurations of the system. The virtual work δW has the same form as the integrand of the work integral with actual differential displacements replaced with virtual variations. Making this replacement to Eq. (3.12), the virtual work can be expressed as

$$\delta W = u\delta\theta \tag{3.13}$$

Since the only control torque is the one applied to the central rigid body, the generalizes force vector $\bar{F}$ can be expressed in matrix form as

$$\bar{F} = \begin{bmatrix} F_1 \\ F_2 \\ F_3 \\ \vdots \\ F_n \end{bmatrix} = \begin{bmatrix} F_\theta \\ F_{y_1} \\ F_{y_2} \\ \vdots \\ F_{y_{\mathcal{A}}} \end{bmatrix} = \begin{bmatrix} 1 \\ 0 \\ 0 \\ \vdots \\ 0 \end{bmatrix} u \tag{3.14}$$

using Eqs. (3.5),(3.7),(3.8),(3.11), and (3.14) in Eq. (3.10) yields the following matrix form

for the system equation of motion:

$$\begin{bmatrix} J_h + M_{\theta\theta} & M_{\theta q}^T \\ M_{\theta q} & M_{qq} \end{bmatrix} \begin{bmatrix} \ddot{\theta} \\ \ddot{\bar{q}} \end{bmatrix} + \begin{bmatrix} 0 & 0 \\ 0 & K_{qq} \end{bmatrix} \begin{bmatrix} \theta \\ \bar{q} \end{bmatrix} = \begin{bmatrix} 1 \\ \bar{0} \end{bmatrix} u \tag{3.15}$$

where the elements of the mass and stiffness matrices are obtained from

$$M_{\theta\theta} = \int_0^L \rho(L_0 + x)^2 \, \mathrm{d}x \tag{3.16a}$$

$$M_{\theta q} = \int_0^L \rho(L_0 + x)\psi_j(x) \, \mathrm{d}x \tag{3.16b}$$

$$M_{qq} = \int_0^L \rho\psi_i(x)\psi_j(x) \, \mathrm{d}x \tag{3.16c}$$

$$K_{qq} = \int_0^L EI\psi_i''(x)\psi_j''(x) \, \mathrm{d}x \tag{3.16d}$$

3.2 Finite Element Method

The finite element method is used to generate the flexible body characteristics for use in a time domain simulation which integrates external forces and moments to the flexible body. FEM is a method of structural and dynamic analysis that enables the numerical integration of a system. Through FEM, the system's mass and stiffness matrices are developed to generate the system's characteristic behavior. In the finite element approach, the system is regarded as an assembly of many geometrically simple discrete elements where, in each element, simple local interpolation functions of motion on the element boundaries are used to model deformations interior to the finite element. The family of piece-wise continuous elements constitutes a finite element model, and the boundary coordinates become

the system's generalized coordinates. In FEM, the admissible functions are local interpolation functions defined over small subdomains usually consist of simple functions such as low-degree polynomials.

To analyze the beam as an element with nodes, an equation for the transverse displacement variation through the length of an element of the beam is chosen to be [1]

$$y(x) = c_1 x^3 + c_2 x^2 + c_3 x + c_4 \tag{3.17}$$

where c_1, c_2, c_3, and c_4 are constants determined such that the function above satisfies the basic beam differential equation and the condition of displacement and slope continuity at nodes shared by two elements [1], i.e.

$$y(0) := d_{1y} = c_4 \tag{3.18a}$$

$$\left.\frac{dy}{dx}\right|_{(x=0)} := \phi_1 = c_3 \tag{3.18b}$$

$$y(l) := d_{2y} = c_1 l^3 + c_2 l^2 + c_3 l + c_4 \tag{3.18c}$$

$$\left.\frac{dy}{dx}\right|_{(x=l)} := \phi_2 = 3c_1 l^2 + 2c_2 l + c_3 \tag{3.18d}$$

By solving for the constants $c_i (i = 1, 2, 3, 4)$ in Eqs. (3.18a)-(3.18d) in terms of the displacements d_{1y} and d_{1y} and slopes ϕ_1 and ϕ_2, and substituting them into Eq. (3.17), the transverse displacement is obtained as

$$y(x) = \left[\frac{2}{l^3}(d_{1y} - d_{2y}) + \frac{1}{l^2}(\phi_1 + \phi_2)\right]x^3 + \left[-\frac{3}{l^2}(d_{1y} - d_{2y}) + \frac{1}{l}(2\phi_1 + \phi_2)\right]x^2 + \phi_1 x + d_{1y} \quad (3.19)$$

which can be expressed in matrix-vector form as

$$y = Nd \quad (3.20)$$

where $d = [d_{1y}, \phi_1, d_{2y}, \phi_2]^T$, $N = [N_1, N_2, N_3, N_4]$, and the interpolation (or shape) functions for the beam element, also known as Hermite cubic interpolation (or cubic spine) functions, are defined as

$$\begin{aligned} N_1 &= \frac{1}{l^3}(2x^3 - 3x^2 l + l^3), \quad N_2 = \frac{1}{l^3}(x^3 l - 2x^2 l^2 + x l^3) \\ N_3 &= \frac{1}{l^3}(-2x^3 + 3x^2 l), \quad N_4 = \frac{1}{l^3}(x^3 l - x^2 l^2) \end{aligned} \quad (3.21)$$

3.2.1 Local Stiffness and Mass Matrices of the Beam

With the interpolation functions acquired for each beam element, the local stiffness and mass matrices for a beam element can be obtained. To derive the local stiffness matrix and equations, a direct equilibrium approach can be used. Relating the nodal and beam theory sign conventions to shear forces and bending moments yields

$$\hat{f}_{1y} = S(0) = EI\frac{d^3y}{dx^3}\Big|_{(x=0)} = \frac{EI}{l^3}(12d_{1y} + 6l\phi_1 - 12d_{2y} + 6l\phi_2) \quad (3.22a)$$

$$\hat{\tau}_1 = -\tau(0) = -EI\frac{d^2y}{dx^2}\Big|_{(x=0)} = \frac{EI}{l^3}(6ld_{1y} + 4l^2\phi_1 - 6ld_{2y} + 2l^2\phi_2) \quad (3.22b)$$

$$\hat{f}_{2y} = -S(l) = -EI\frac{d^3y}{dx^3}\Big|_{(x=l)} = \frac{EI}{l^3}(-12d_{1y} - 6l\phi_1 + 12d_{2y} - 6l\phi_2) \tag{3.22c}$$

$$\hat{\tau}_2 = \tau(l) = EI\frac{d^2y}{dx^2}\Big|_{(x=l)} = \frac{EI}{l^3}(6ld_{1y} + 2l^2\phi_1 - 6ld_{2y} + 4l^2\phi_2) \tag{3.22d}$$

where $\hat{f_{iy}}$ and $\hat{\tau}_i$ are the local forces and moments, respectively, at each end of a beam element. Eqs. (3.22a)-(3.22d) can be rewritten in matrix form as

$$F = kd \tag{3.23}$$

where $F = [F_1^T, F_2^T]^T$, $F_i = [\hat{f}_{iy}, \hat{\tau}_i]^T (i = 1, 2)$, and the local stiffness matrix for each element is given by

$$k = \frac{EI}{l^3}\begin{bmatrix} 12 & 6l & -12 & 6l \\ 6l & 4l^2 & -6l & 2l^2 \\ -12 & -6l & 12 & -6l \\ 6l & 2l^2 & -6l & 4l^2 \end{bmatrix} \tag{3.24}$$

The dynamic analysis of the system uses a consistent-mass matrix for a more accurate depiction of the system. To develop the local mass matrix equation for a beam element, D'Alembert's principle is used. By utilizing the shape functions used to obtain the local stiffness matrix, the local mass matrix is obtained as

$$m = \int_0^l \rho N^T N \, \mathrm{d}x \tag{3.25}$$

where ρ is the mass per unit length and is assumed to be constant. Substituting the shape functions in Eq. (3.21) into Eq. (3.25) yields

$$m = \frac{\rho l}{420}\begin{bmatrix} 156 & 22l & 54 & -13l \\ 22l & 4l^2 & 13l & -3l^2 \\ 54 & 13l & 156 & -22l \\ -13l & -3l^2 & -22l & 4l^2 \end{bmatrix} \tag{3.26}$$

3.2.2 Application of FEM to the Rigid-Flexible System

In this section, FEM is applied to the rigid-flexible system to transform the partial differential equations of motion into a finite-dimensional set of second-order differential equations in terms of the displacements, velocities, and accelerations of the finite element coordinates, and the external forcing functions [33]. The total transverse velocity (of a mass element on the beam) is given by

$$v(x,t) = \dot{y}(x,t) + (x + L_0)\dot{\theta}(t) \tag{3.27}$$

where x is measured from the outer radius of the hub along the undeformed appendage axis. Assuming Euler-Bernoulli beam theory and small deformation, the kinetic energy and potential energy are expressed, respectively, as

$$T = \frac{1}{2}J_h\dot{\theta}^2 + \frac{1}{2}\int_0^L \rho v^2 \, \mathrm{d}x \tag{3.28}$$

and

$$U = \frac{1}{2}\int_0^L EI\left(\frac{d^2y}{dx^2}\right)^2 \mathrm{d}x \tag{3.29}$$

where J_h is the moment of inertia of the central rigid body. The virtual work done by the external torque u is given by

$$\delta W_{nc} = u\delta\theta(t) \tag{3.30}$$

Applying the extended Hamilton's principle with Eqs. (3.28)-(3.30) yields

$$\int_{t_1}^{t_2}\left[J_h\dot{\theta}\delta\dot{\theta}+\int_0^L \rho(\delta\dot{y}+(x+L_0)\delta\dot{\theta})(\dot{y}+(x+L_0)\dot{\theta})\,\mathrm{d}x+\int_0^L EI\left(\frac{\partial^2 y}{\partial x^2}\right)\delta\left(\frac{\partial^2 y}{\partial x^2}\right)\mathrm{d}x+u\delta\theta\right]\mathrm{d}t=0 \tag{3.31}$$

Through integration by parts and some manipulations to collect the δy and $\delta\theta$ terms, Eq. (3.31) is transformed into

$$\begin{aligned}\int_{t_1}^{t_2}\Bigg[\int_0^L\left(\rho(\ddot{y}+(x+L_0)\ddot{\theta})\delta y+EI\left(\frac{\partial^2 y}{\partial x^2}\right)\delta\left(\frac{\partial^2 y}{\partial x^2}\right)\right)\mathrm{d}x \\ +\left(\int_0^L \rho(x+L_0)(\ddot{y}+(x+L_0)\ddot{\theta})\,\mathrm{d}x+J_h\ddot{\theta}-u\right)\delta\theta\Bigg]\mathrm{d}t=0\end{aligned} \tag{3.32}$$

The displacement $y(x,t)$ can be discretized using the finite element expansion

$$y(x,t)=\sum_{i=1}^{4}N_i^{(e)}(x)d_i^{(e)}(t)\qquad(i=1,2,3,4) \tag{3.33}$$

where $N_i^{(e)}(x)$ are the interpolation functions from Eq. (3.21) for any beam element e ($e=1,2,...,n$) and d_i are the nodal displacements. The acceleration and curvature are expressed as

$$\ddot{y}(x,t)=\sum_{i=1}^{4}N_i^{(e)}(x)\ddot{d}_i^{(e)}(t)\qquad(i=1,2,3,4) \tag{3.34}$$

$$\frac{\partial^2 y}{\partial x^2}=\sum_{i=1}^{4}\frac{\partial^2}{\partial x^2}\Big(N_i^{(e)}(x)\Big)d_i^{(e)}(t)\qquad(i=1,2,3,4) \tag{3.35}$$

Substitution of Eqs. (3.33)-(3.35) into Eq. (3.32) and integration over the spatial domains leads to the global mass, stiffness, and forcing matrices. The assembled set of matrix differential equations is as follows:

$$\begin{bmatrix} J_h + M_{\theta\theta} & M_{\theta d} \\ M_{\theta d}^T & M_{dd} \end{bmatrix} \begin{bmatrix} \ddot{\theta} \\ \ddot{\bar{d}} \end{bmatrix} + \begin{bmatrix} 0 & 0 \\ 0 & K_{dd} \end{bmatrix} \begin{bmatrix} \theta \\ \bar{d} \end{bmatrix} = \begin{bmatrix} 1 \\ \bar{0} \end{bmatrix} u \tag{3.36a}$$

where

$$M_{\theta\theta} = \sum_{e=1}^{n} M_{11}^{(e)} \tag{3.36b}$$

$$M_{\theta d} = \begin{bmatrix} M_{13}^{(1)} + M_{12}^{(2)}, & M_{13}^{(2)} + M_{12}^{(3)}, & M_{13}^{(3)} + M_{12}^{(4)}, & \ldots, & M_{13}^{(n-1)} + M_{12}^{(n)}, & M_{13}^{(n)} \end{bmatrix} \tag{3.36c}$$

$$M_{dd} = \begin{bmatrix} M_{33}^{(1)} + M_{22}^{(2)} & M_{32}^{(2)} & & & & & \\ M_{32}^{(2)} & M_{33}^{(2)} + M_{22}^{(3)} & M_{23}^{(3)} & & & & \\ & M_{32}^{(3)} & M_{33}^{(3)} + M_{22}^{(4)} & M_{23}^{(4)} & & & \\ & & M_{32}^{(4)} & \ddots & & & \\ & & & M_{32}^{(n-1)} & M_{33}^{(n-1)} + M_{22}^{(n)} & M_{23}^{(n)} & \\ & & & & M_{32}^{(n)} & M_{33}^{(n)} & \end{bmatrix} \tag{3.36d}$$

$$K_{dd} = \begin{bmatrix} K_{33}^{(1)} + K_{22}^{(2)} & K_{32}^{(2)} & & & & & \\ K_{32}^{(2)} & K_{33}^{(2)} + K_{22}^{(3)} & K_{23}^{(3)} & & & & \\ & K_{32}^{(3)} & K_{33}^{(3)} + K_{22}^{(4)} & K_{23}^{(4)} & & & \\ & & K_{32}^{(4)} & \ddots & & & \\ & & & K_{32}^{(n-1)} & K_{33}^{(n-1)} + K_{22}^{(n)} & K_{23}^{(n)} & \\ & & & & K_{32}^{(n)} & K_{33}^{(n)} & \end{bmatrix} \tag{3.36e}$$

and the local stiffness and mass matrices from Eqs. (3.24) and (3.26), respectively, for each element are used to obtain the beam's global stiffness and mass matrices. Imposing the

boundary conditions on these global matrices produces M_{dd} and K_{dd}. The submatrix elements are defined as

$$M^{(e)} = \begin{bmatrix} M_{11}^{(e)} & M_{12}^{(e)} & M_{13}^{(e)} \\ M_{21}^{(e)} & M_{22}^{(e)} & M_{23}^{(e)} \\ M_{31}^{(e)} & M_{32}^{(e)} & M_{33}^{(e)} \end{bmatrix}, \quad K^{(e)} = \begin{bmatrix} 0 & 0 & 0 \\ 0 & K_{22}^{(e)} & K_{23}^{(e)} \\ 0 & K_{32}^{(e)} & K_{33}^{(e)} \end{bmatrix} \qquad (e = 1, 2, \ldots, n)$$

where

$$M_{11}^{(e)} = \frac{\rho l}{3}\left((x_e + L_0)^2 + (x_e + L_0 + l)(x_e + L_0)^2 + (x_e + L_0 + l)^2\right)$$

$$M_{12}^{(e)} = M_{21}^{(e)\ T} = \rho l \left[\tfrac{3}{20}l + \tfrac{1}{2}(x_e + L_0), \quad \tfrac{1}{30}l + \tfrac{1}{12}l(x_e + L_0)\right]$$

$$M_{13}^{(e)} = M_{31}^{(e)\ T} = \rho l \left[\tfrac{7}{20}l + \tfrac{1}{2}(x_e + L_0), \quad -\tfrac{1}{20}l - \tfrac{1}{12}l(x_e + L_0)\right]$$

$$M_{22}^{(e)} = \frac{\rho l}{420}\begin{bmatrix} 156 & 22l \\ 22l & 4l^2 \end{bmatrix}$$

$$M_{23}^{(e)} = M_{32}^{(e)\ T} = \frac{\rho l}{420}\begin{bmatrix} 54 & -13l \\ -13l & -3l^2 \end{bmatrix}$$

$$M_{33}^{(e)} = \frac{\rho l}{420}\begin{bmatrix} 156 & -22l \\ -22l & 4l^2 \end{bmatrix}$$

and

$$K_{22}^{(e)} = \frac{EI}{l^3}\begin{bmatrix} 12 & 6l \\ 6l & 4l^2 \end{bmatrix}$$

$$K_{23}^{(e)} = K_{32}^{(e)\ T} = \frac{EI}{l^3}\begin{bmatrix} -12 & 6l \\ -6l & 2l^2 \end{bmatrix}$$

$$K_{33}^{(e)} = \frac{EI}{l^3}\begin{bmatrix} 12 & -6l \\ -6l & 4l^2 \end{bmatrix}$$

and where x_e is the distance from the root of the appendage to the left end of the e^{th} finite element, L_0 is the radius of the hub, l is the length of the finite element, and ρ is the constant mass per unit length of the beam.

3.3 Inclusion of Beam Damping

Along with the global mass and stiffness matrices, the damping effect is also considered. For this system, proportional, or Rayleigh, damping is considered. The global damping matrix utilizes the global mass and stiffness matrices, each multiplied by a proportional constant, α and β, i.e.,

$$D = \alpha M + \beta K :\rightarrow M\ddot{x} + D\dot{x} + Kx = Fu \tag{3.38}$$

From Eq. (3.38), the eigenvalue problem of the homogeneous form

$$(M\lambda^2 + D\lambda + K)\bar{\Phi} = \bar{0}, \qquad \lambda = -\sigma + j\Omega, \tag{3.39}$$

where σ is the damping decay constant, and Ω is the damped natural frequency, can be obtained. Solving the eigenvalue yields

$$(M\lambda^2 + (\alpha M + \beta K)\lambda + K)\bar{\Phi} = \bar{0} \tag{3.40}$$

$$\big(M((\sigma^2 - \Omega^2 - \alpha\sigma) + j(-2\sigma\Omega + \alpha\Omega)) + K((-\sigma\beta + 1) + j\beta\Omega)\big)\bar{\Phi} = \bar{0} \tag{3.41}$$

The real and imaginary parts of Eq. (3.41) can be separated, respectively, i.e.,

$$\big(M(\sigma^2 - \Omega^2 - \alpha\sigma) + K(-\sigma\beta + 1)\big)\bar{\Phi} = \bar{0} \tag{3.42a}$$

$$\left(\frac{(\sigma^2 - \Omega^2 - \alpha\sigma)}{-\sigma\beta + 1}M + K\right)\bar{\Phi} = \bar{0} \tag{3.42b}$$

and

$$\big(M(-2\sigma\Omega + \alpha\Omega) + K(\beta\Omega)\big)\bar{\Phi} = \bar{0} \tag{3.43a}$$

$$\left(\frac{(-2\sigma + \alpha)}{\beta}M + K\right)\bar{\Phi} = \bar{0} \tag{3.43b}$$

From real and imaginary parts, each eigenvalue, or pole, is found

$$\frac{(\sigma_i^2 - \Omega_i^2 - \alpha\sigma_i)}{-\sigma_i\beta + 1} = \frac{(-2\sigma_i + \alpha)}{\beta} = -\omega_{n_i}^2 \tag{3.44}$$

where $\omega_{n_i}^2 = \sigma_i^2 + \Omega_i^2$ is the undamped natural frequency squared. With the first two non-zero circular natural frequencies and two specified damping ratios, $\zeta = \sigma/\omega_n$, α and β can be found from

$$\alpha + \beta\omega_{n_i}^2 = 2\omega_{n_i}\zeta_i \ , \quad (i = 1, 2) \tag{3.45}$$

where

$$\alpha = \frac{2\omega_{n_1}\omega_{n_2}}{\omega_{n_2}^2 - \omega_{n_1}^2}(\omega_{n_2}\zeta_1 - \omega_{n_1}\zeta_2), \tag{3.46}$$

and

$$\beta = \frac{2}{\omega_{n_2}^2 - \omega_{n_1}^2}(\omega_{n_2}\zeta_2 - \omega_{n_1}\zeta_1) \tag{3.47}$$

Once the global damping matrix D is obtained from Eq. (3.38), it is included in the final set of vector-matrix differential equations for the assumed modes method,

$$\begin{bmatrix} J_h + M_{\theta\theta} & M_{\theta q}^T \\ M_{\theta q} & M_{qq} \end{bmatrix} \begin{bmatrix} \ddot{\theta} \\ \ddot{\bar{q}} \end{bmatrix} + \begin{bmatrix} \alpha M_{\theta\theta} & \alpha M_{\theta q}^T \\ \alpha M_{\theta q} & \alpha M_{qq} + \beta K_{qq} \end{bmatrix} \begin{bmatrix} \dot{\theta} \\ \dot{\bar{q}} \end{bmatrix} + \begin{bmatrix} 0 & 0 \\ 0 & K_{qq} \end{bmatrix} \begin{bmatrix} \theta \\ \bar{q} \end{bmatrix} = Fu \tag{3.48}$$

and the finite element method,

$$\begin{bmatrix} J_h + M_{\theta\theta} & M_{\theta d} \\ M_{\theta d}^T & M_{dd} \end{bmatrix} \begin{bmatrix} \ddot{\theta} \\ \ddot{\bar{d}} \end{bmatrix} + \begin{bmatrix} \alpha M_{\theta\theta} & \alpha M_{\theta d} \\ \alpha M_{\theta d}^T & \alpha M_{dd} + \beta K_{dd} \end{bmatrix} \begin{bmatrix} \dot{\theta} \\ \dot{\bar{d}} \end{bmatrix} + \begin{bmatrix} 0 & 0 \\ 0 & K_{dd} \end{bmatrix} \begin{bmatrix} \theta \\ \bar{d} \end{bmatrix} = Fu \tag{3.49}$$

3.4 Formulation Method Comparison

The nonlinear ordinary and partial differential equations of motion of the rigid-flexible system in Eqs. (2.9a), (2.9b), and (2.9c) have been linearized into a set of vector-matrix

differential equations shown in Eqs. (3.48) and (3.49) from the assumed modes method and finite element method, respectively. Both methods provided linearized approximations of the nonlinear model that also include the rigid-flexible coupled dynamics. Although at first glance they may seem to have produced identical equations of motion, there are several underlying qualitative differences that can have a significant impact when it comes to simulation and practical application.

The admissible functions of the assumed modes method are global functions defined over the entire domain of the system. These functions are often complicated and require complex derivation and analysis in order to accurately represent the entire system. The finite element method, instead, uses local admissible functions defined over small subdomains that constitute the whole system, which allows for simple and low-degree polynomials to be chosen in conjunction with the element boundaries. However, because the element boundaries are used to model deformations interior to the finite element, the boundary coordinates of each element become the system's generalized coordinates, which results in a high order system.

The assumed modes method utilizes time-dependent amplitude functions as the generalized coordinates, which typically results in lower order systems. It is important, however, to recall that the generalized coordinates from the assumed modes method are not explicitly correlated to the propagated motion of the flexible structure. The actual deformation of the flexible structure at each location along the length of the beam requires a summation of all the amplitude functions multiplied with the space-dependent admissible functions. The generalized coordinates from the finite method represent physical coordinates. Finally, the assumed modes method is generally applicable for problems with simple geometry and often require a new set of functions for each new problem, unlike the finite element method that can be broadly applicable to arbitrary geometries and can typically use the similar low-degree polynomial functions. Therefore, the linearized equations of motion derived from the finite element method are considered for control design and simulation.

4 Stability Analysis and Control Design

If an open-loop system is found to be naturally unstable, a control law may be applied to guarantee stability of the new closed-loop system. However, if no control law is capable of stabilizing the system, the system model and equations of motion may require a re-evaluation, especially in the case of the linearization of a nonlinear system.

The control laws designed and applied to the rigid-flexible system are all closed-loop, feedback control laws with the following control objectives:

- Begin at some arbitrary initial condition.
- Rotate the central rigid body to a new, desired angular position and with a zero final angular velocity.
- Suppress vibration of flexible appendage during motion and reduce flexural deformation to zero in the final position.

4.1 System Stability

Two general methods of stability analysis are introduced and summarized in this section: Lyapunov's indirect method and Lyapunov's direct method. Lyapunov's indirect method serves to study the stability of the open-loop system. Lyapunov's direct method provides a control law that guarantees asymptotic stability for the closed-loop form of the rigid-flexible system.

4.1.1 Lyapunov's Indirect Method

One method of determining the stability of a linear time-invariant system is by studying the eigenvalues of the system. The linearized equations of motion of the rigid-flexible system in Eqs. (3.48) and (3.49) can be rewritten in a state-space representation as

$$\dot{X}(t) = AX(t) + Bu(t) = \begin{bmatrix} 0_{p\times p} & I_p \\ -M^{-1}K & -M^{-1}D \end{bmatrix} X(t) + \begin{bmatrix} 0_{p\times 1} \\ M^{-1}F \end{bmatrix} u(t) \tag{4.1a}$$

$$Y(t) = CX(t) \tag{4.1b}$$

where $X(t) = [\theta, \bar{d}^T, \dot{\theta}, \dot{\bar{d}}^T]^T \in \mathbb{R}^{2p}$ $(p = 2e + 1)$ is the augmented state variable vector, $Y(t) \in \mathbb{R}^g$ is the output or measurement vector for g outputs, $A \in \mathbb{R}^{2p\times 2p}$ is the state matrix, $B \in \mathbb{R}^{2p\times r}$ is the input matrix, and $C \in \mathbb{R}^{g\times 2p}$ is the output or measurement matrix. The output matrix C is generally defined as as $C = [I_p \ 0_{p\times p}]$ in Eq. (4.1b) because only the position state variables are generally measurable. However, when assuming a full-state system, all of the state variables are assumed to be measurable, redefining the output matrix as $C = I_{2p}$. However, . The eigenvalues, $\{\lambda_i\}$ $(i = 1, \ldots, 2p)$, of the system in Eq. (4.1a) are determined by solving for the roots of the characteristic polynomial obtained from taking the determinant of $\lambda I - A$, i.e.,

$$\det(\lambda I - A) = 0 \tag{4.2}$$

The stability of the linear time-invariant system can then be determined by analyzing its eigenvalues under the following criteria [40]:

- The system is asymptotically stable if and only if $\mathrm{Re}(\lambda_i) < 0$ for all λ_i.
- The system is stable if and only if $\mathrm{Re}(\lambda_i) \leq 0$ for all simple or semi-simple λ_i and $\mathrm{Re}(\lambda_i) < 0$ for all nonsemi-simple λ_i.
- The system is unstable if and only if $\mathrm{Re}(\lambda_i) > 0$ for any simple or semi-simple λ_i and $\mathrm{Re}(\lambda_i) \geq 0$ for any nonsemi-simple λ_i.

4.1.2 Lyapunov's Direct Method

Stability analysis of the rigid-flexible system can also be performed with the direct Lyapunov method, which requires only the form of the differential equations to be known. Lyapunov's direct method utilizes a scalar function of the states similar to a generalized energy of the system and is called the Lyapunov function $\mathcal{V}(\bar{x})$. Consider a single valued continuously differentiable function $\mathcal{V}(\bar{x})$ such that $\mathcal{V}(\bar{0}) = 0$ and in some region $\mathcal{D}$ around the system equilibrium $\bar{x} = \bar{0}$. Although it is not necessarily the case here, it is important to note if the equilibrium is not at the origin, the system can be translated to an equivalent system with equilibrium at the origin. The following theorems explain the stability of the system about the equilibrium point through the Lyapunov function.

Theorem 4.1. If a positive definite function $\mathcal{V}(\bar{x})$ $(\mathcal{V}(\bar{x}) > 0 \ \forall \bar{x} \neq \bar{0} \in \mathcal{D})$ can be determined such that $\dot{\mathcal{V}}(\bar{x})$ is negative semidefinite $(\dot{\mathcal{V}}(\bar{x}) \leq 0)$, then the origin is locally stable in the neighborhood $\mathcal{D}$ of the origin.

Theorem 4.2. If a positive definite function $\mathcal{V}(\bar{x})$ $(\mathcal{V}(\bar{x}) > 0 \ \forall \bar{x} \neq \bar{0} \in \mathcal{D})$ can be determined such that $\dot{\mathcal{V}}(\bar{x})$ is negative definite $(\dot{\mathcal{V}}(\bar{x}) < 0)$, then the origin is locally asymptotically stable in the neighborhood $\mathcal{D}$ of the origin.

Theorem 4.3. If a positive definite function $\mathcal{V}(\bar{x})$ $(\mathcal{V}(\bar{x}) > 0 \ \forall \bar{x} \neq \bar{0} \in \mathcal{D})$ can be determined such that $\dot{\mathcal{V}}(\bar{x})$ is negative definite for all $\bar{x} \neq \bar{0}$ and $\mathcal{V}(\bar{x}) \to \infty$ as $||\bar{x}|| \to \infty$, then the origin is globally asymptotically stable.

4.2 Observabilty and Controllability

A linear system is said to be observable at some time t if $x(t)$ can be determined from the output function $y(t)$. If this is true for all t and $x(t)$, then the system is considered fully observable. The observability is a major requirement in filtering and state estimation problems. Many feedback control laws that require knowledge of the states often rely on the output variables instead for feedback signals. If the system is observable, then y contains sufficient information about the internal states so that most of the power of the state feedback can still be realized [40].

The LTI system in Eqs. (4.1a) and (4.1b) is considered observable if and only if any of the following equivalent conditions is satisfied [41]:

- The observability Grammian $W_O(t) := \int_{t_0}^{t} e^{A^T\tau} C^T C e^{A\tau}\, \mathrm{d}\tau$ is positive definite and invertible for all $t > 0$.
- The columns of Ce^{At} are linearly independent for all $t > 0$.
- The columns of $C(sI - A)^{-1}$ are linearly independent.
- The observability matrix

$$P_O = \begin{bmatrix} C^T & \vdots & (CA)^T & \vdots & (CA^2)^T & \vdots & \cdots & \vdots & (CA^{n-1})^T \end{bmatrix}^T \in \mathbb{R}^{2pg \times 2p} \tag{4.3}$$

  has full rank, i.e. rank $= 2p$.

- The matrix $\begin{bmatrix} \lambda_i I - A \\ C \end{bmatrix}$ has full rank for every eigenvalue of A; therefore, the matrix $\begin{bmatrix} sI - A \\ C \end{bmatrix}$ has full rank for all values of s.
- If the matrix A is Hurwitz, i.e., stable with negative real-part eigenvalues, then there is a unique positive definite solution W to the Lyapunov equation $A^T W + WA = -C^T C$ given by $W = W_O(\infty)$

If the linear system is not fully observable, it may still be detectable. A system is detectable if the unobservable states are asymptotically stable. The detectability of a system can be determined by checking if

$$\mathrm{rank}\left(\begin{bmatrix} \lambda_i I - A \\ C \end{bmatrix} \right) = 2p \tag{4.4}$$

for all $Re\ (\lambda_i) \geq 0$.

A linear system is said to be controllable at t_0 if it is possible to find some input function $u(t)$, defined over $t \in \mathcal{T}$, which will transfer the initial state $x(t_0)$ to the origin at some finite time $t_1 \in \mathcal{T}$, $t_1 > t_0$. That is, there exists some input $u_{[t_0,t_1]}$, which gives $x(t_1) = 0$ at a finite time $t_1 \in \mathcal{T}$. If this is true for all initial times and all initial states, the system is completely controllable. If the system is not completely controllable, then for some initial states no input exists which can drive the system to the zero state. If a linear system is controllable, it is possible to design a state feedback control law with specified closed-loop eigenvalues. Thus, an unstable system can be stabilized, a slow system can be sped up, the natural frequencies can be changed, etc.

The LTI system in Eqs. (4.1a) and (4.1b) is considered observable if and only if any of the following equivalent conditions is satisfied [41]:

- The controllability Grammian $W_C(t) := \int_{t_0}^{t} e^{A\tau} B B^T e^{A^T \tau} \, \mathrm{d}\tau$ is positive definite and invertible for all $t > 0$.
- The columns of $e^{At}B$ are linearly independent for all $t > 0$.
- The columns of $(sI - A)^{-1}B$ are linearly independent.
- The controllability matrix

$$P_C = \begin{bmatrix} B & \vdots & AB & \vdots & A^2B & \vdots & \cdots & \vdots & A^{n-1}B \end{bmatrix} \in \mathbb{R}^{2p \times 2pr} \tag{4.5}$$

  has full rank, i.e. rank $= 2p$.
- The matrix $\begin{bmatrix} \lambda_i I - A & B \end{bmatrix}$ has full rank for every eigenvalue of A; therefore, the matrix $\begin{bmatrix} sI - A & B \end{bmatrix}$ has full rank for all values of s.
- If the matrix A is Hurwitz, i.e. stable with negative real-part eigenvalues, then there is a unique positive definite solution W to the Lyapunov equation $A^T W + W A = -BB^T$ given by $W = W_C(\infty)$

If the linear system is not completely controllable, it may still be stabilizable. A system is stabilizable if all unstable states are controllable and all uncontrollable states are already stable. The stabilizability of a system can be determined by checking if

$$\text{rank}\left(\begin{bmatrix} \lambda_i I - A & B \end{bmatrix} \right) = 2p \tag{4.6}$$

for all $Re\ (\lambda_i) \geq 0$.

4.3 State-Feedback Control Design

A control system is defined as any system which exists for the purpose of regulating or controlling the flow of information or data in some desired fashion to yield a desired result. Two general classes of control systems are open-loop and closed-loop systems. The control input $u(t)$ for an open-loop system is selected based on the goals for the system and all available a priori knowledge about the system. It is in no way influenced by the output $y(t)$ of the system. Therefore, if unexpected disturbances act upon an open-loop system, or the behavior of the system is not completely understood, then the output will not behave precisely as expected or desired [40]. On the other hand, a closed-loop, or feedback, control system utilizes a control input that is modified in some way by the information about the behavior of the system output. A feedback system is often better able to deal with unexpected disturbances and uncertainties about the system's dynamic behavior. However, it is important to keep in mind that closed-loop control is not always superior to open-loop.

In this section, the state-feedback control laws are designed with the assumption that all of the state variables are measurable and contain all pertinent information about the system. Note that this assumption is not always the case in real-life application as only some states are measurable depending on the available output sensors. State-estimation for such cases are also considered and designed later on in the chapter.

4.3.1 Lyapunov-Based Control Law

With Lyapunov's direct method in mind, the stability of the rigid-flexible system has already been determined through the application of a Lyapunov candidate function [33]. Utilizing a generalized energy equation $E = T + U$ where T and U are given in Eqs. (3.28) and (3.29), the following Lyapunov candidate function

$$2\mathcal{V} = a_1 J_h \left(\frac{d\theta}{dt}\right)^2 + a_2(\theta - \theta_f)^2 + a_3 \left[\int_{L_0}^{L} \rho(\dot{y} + x\dot{\theta})^2 \,\mathrm{d}x + \int_{L_0}^{L} EI\left(\frac{\partial^2 y}{\partial x^2}\right)^2 \mathrm{d}x\right] \tag{4.7}$$

is positive-definite and zero only at the desired states ($\theta = \theta_f$ rad/s and $\frac{d\theta_f}{dt} = 0$ rad/s^2) [33, 34]. The time derivative of the Lyapunov function in Eq. (4.7) is first taken.

$$\begin{aligned} 2\frac{d\mathcal{V}}{dt} =& 2a_1 J_h \left(\frac{d\theta}{dt}\right)\left(\frac{d^2\theta}{dt^2}\right) + 2a_2(\theta - \theta_f)\left(\frac{d\theta}{dt}\right) \\ &+ a_3 \left[2\int_{L_0}^{L} \rho(\dot{y} + x\dot{\theta})(\ddot{y} + x\ddot{\theta}) \,\mathrm{d}x + \frac{d}{dt}\int_{L_0}^{L} EI\left(\frac{\partial^2 y}{\partial x^2}\right)^2 \mathrm{d}x\right] \end{aligned} \tag{4.8}$$

The partial differential equations of the rigid-flexible body system from Eqs. (2.9a) and (2.9a) are then substituted into Eq. (4.8). replacing the angular acceleration such that

$$\begin{aligned} 2\frac{d\mathcal{V}}{dt} =& 2a_1 \left(\frac{d\theta}{dt}\right)\left(u - \int_{L_0}^{L} \rho x(\ddot{y} + x\ddot{\theta}) \,\mathrm{d}x\right) + 2a_2(\theta - \theta_f)\left(\frac{d\theta}{dt}\right) \\ &+ a_3 \left[2\int_{L_0}^{L} \rho(\dot{y} + x\dot{\theta})(\ddot{y} + x\ddot{\theta}) \,\mathrm{d}x + \frac{d}{dt}\int_{L_0}^{L} EI\left(\frac{\partial^2 y}{\partial x^2}\right)^2 \mathrm{d}x\right] \end{aligned} \tag{4.9}$$

By taking Eq. (2.9c), multiplying x throughout, and integrating over the space domain from L_0 to L, i.e,

$$-\int_{L_0}^{L} \rho x(\ddot{y} + x\ddot{\theta}) \,\mathrm{d}x = \int_{L_0}^{L} xEI\frac{\partial^4 y}{\partial x^4} \,\mathrm{d}x \tag{4.10}$$

Eq. (4.10) can be substituted into Eq. (4.9),

$$\begin{aligned} 2\frac{d\mathcal{V}}{dt} =& 2a_1\left(\frac{d\theta}{dt}\right)\left(u+\int_{L_0}^{L} xEI\left(\frac{\partial^2 y}{\partial x^2}\right)^2 \mathrm{d}x\right) + 2a_2(\theta-\theta_f)\left(\frac{d\theta}{dt}\right) \\ &+ a_3\left[2\int_{L_0}^{L}\rho(\dot{y}+x\dot{\theta})(\ddot{y}+x\ddot{\theta})\,\mathrm{d}x + \frac{d}{dt}\int_{L_0}^{L} EI\left(\frac{\partial^2 y}{\partial x^2}\right)^2 \mathrm{d}x\right] \end{aligned} \tag{4.11}$$

Once again, recall Eq. (2.9c). After multiplying $(\dot{y}+x\dot{\theta})$ throughout Eq.(2.9c), the first integral in the brackets in Eq.(4.11) can be rewritten as

$$\int_{L_0}^{L}\rho(\dot{y}+x\dot{\theta})(\ddot{y}+x\ddot{\theta})\,\mathrm{d}x = -\int_{L_0}^{L} EI\frac{\partial^4 y}{\partial x^4}(\dot{y}+x\dot{\theta})\,\mathrm{d}x \tag{4.12}$$

Through integration by parts, the right-hand side of Eq. (4.12) can be simplified to

$$\begin{aligned} \int_{L_0}^{L}\rho(\dot{y}+x\dot{\theta})(\ddot{y}+x\ddot{\theta})\,\mathrm{d}x =& -\int_{L_0}^{L} EI\frac{\partial^4 y}{\partial x^4}(\dot{y}+x\dot{\theta})\,\mathrm{d}x \\ =& -\int_{L_0}^{L} EI(\dot{y}\frac{\partial^4 y}{\partial x^4}+x\dot{\theta}\frac{\partial^4 y}{\partial x^4})\,\mathrm{d}x \\ =& 0-(\tau_0-L_0S_0)\dot{\theta} \end{aligned} \tag{4.13}$$

Substituting Eq. (4.13) into Eq. (4.11) produces the final time-derivative of the Lyapunov function as

$$2\frac{d\mathcal{V}}{dt} = 2a_1\left(\frac{d\theta}{dt}\right)\left(u+(\tau_0-L_0S_0)\right) + 2a_2(\theta-\theta_f)\left(\frac{d\theta}{dt}\right) + a_3\left[-2(\tau_0-L_0S_0)\left(\frac{d\theta}{dt}\right)\right] \tag{4.14}$$

where the Lyapunov-based control law is defined as

$$u = \left(-\frac{1}{a_1} \right) [-\tilde{u} + a_2(\theta - \theta_f) + (a_3 - a_1)(L_0 S_0 - \tau_0)], \tag{4.15}$$

and $\tilde{u}$ is a freely assignable part of the control torque u. The weighting gains a_i are positive scalar constants that allow relative emphasis on the three contributors to the error of the system. To guarantee asymptotic stability, the time-derivative of the Lyapunov function $\frac{d\mathcal{V}}{dt}$ can be forced to be negative definite if $\tilde{u}$ is selected as

$$\tilde{u} = -a_4 \left(\frac{d\theta}{dt} \right), \quad a_4 > 0. \tag{4.16}$$

The term $(L_0 S_0 - \tau_0)$ denotes the moment, or torque, about the center of rotation of the rigid body due to the vibration of the flexible beam, where τ_0 and S_0 are obtained by substituting Eq. (3.20) into the moment and shear force equations, respectively, i.e.,

$$\tau|_{x=L_0} = \tau_0 = EIGd \tag{4.17}$$

and

$$S|_{x=L_0} = S_0 = EIHd \tag{4.18}$$

where

$$G = \frac{d^2 N}{dx^2} = \left[\frac{12x - 6l}{l^3} \quad \frac{6xl - 4l^2}{l^3} \quad \frac{-12x + 6l}{l^3} \quad \frac{6xl - 2l^2}{l^3} \right] \tag{4.19}$$

and

$$H = \frac{d^3 N}{dx^3} = \left[\frac{12}{l^3} \quad \frac{6l}{l^3} \quad \frac{-12}{l^3} \quad \frac{6l}{l^3} \right]. \tag{4.20}$$

4.3.2 Linear Quadratic Regulator

One of the fundamental design objectives of state-feedback control is the achievement of suitable pole locations to ensure satisfactory transient response while ensuring a stable

system. What constitutes as a suitable pole location depends upon the design specifications regarding relative stability, response times, accuracy, etc. Some optimal control laws also stem from state-feedback control and often take a similar form. For a state-feedback control law, the control input u is defined as

$$u(t) = -K_g X(t) + r(t) \tag{4.21}$$

where K_g is the constant state-feedback gain matrix, and $r(t)$ is some reference input for tracking a desired state. The regulation of a linear system with the goal of minimizing a defined quadratic cost function is also known as a linear quadratic regulator (LQR). To obtain an optimal gain matrix that provides a minimal cost requirement, a quadratic cost function J for the continuous time system is first defined as

$$J = \int_0^\infty (X^T(t)QX(t) + u^T(t)Ru(t) + 2X^T(t)Nu(t))\,\mathrm{d}t \tag{4.22}$$

where Q, R, and N are symmetric weighting matrices that are predetermined according to the desired form of optimization. Solving for the positive-definite solution S of the associated algebraic Riccati equation

$$A^T S + SA - (SB + N)R^{-1}(B^T S + N) + Q = 0 \tag{4.23}$$

results in an asymptotically stable closed-loop system [42] where the state-feedback gain matrix is found to be

$$K_g = R^{-1}(B^T S + N). \tag{4.24}$$

When applying the LQR, several conditions must be satisfied. The pair (A, B) must be at least stabilizable. $Q \geq 0$, $R > 0$, $N \geq 0$, and $Q - NR^{-1}N^T \geq 0$. $(Q - NR^{-1}N^T, A - BR^{-1}N^T)$ must also have no unobservable mode on the imaginary axis.

4.3.3 Sliding Mode Control

The control laws designed up until this point are capable of achieving the control objectives and guaranteeing stability in the system; however, this is only true for an ideal system without any model uncertainties. A more robust control of the rigid-flexible system model is required to compensate for any uncertain terms that enter the state equation at the same point as the control input [43]. These uncertain terms that occur at the same order of differentiation as the control inputs are known as matched uncertainties. In some cases, the uncertain dynamics are not directly coupled to the control input. In fact, if the system under consideration presents these unmatched disturbances, the system trajectories may not converge about any known fixed point [44]. In SMC, trajectories starting off a sliding manifold are forced to reach the manifold in a finite time and to stay on the manifold for all future time. This is known as the reaching phase and is followed by the sliding phase, during which the motion is confined to the manifold. This makes SMC optimal as a robust control law because the motion on the manifold is independent of any matched uncertainties. In this section, a CSMC with a conventional sliding manifold is first introduced to summarize the general SMC theory.

Conventional Sliding Mode Control

Consider a general second-order system

$$\begin{aligned} \dot{x}_1 &= x_2 \\ \dot{x}_2 &= \mathfrak{h}(x) + \mathfrak{g}(x)u \end{aligned} \tag{4.25}$$

where $\mathfrak{h}$ and $\mathfrak{g}$ are unknown nonlinear functions and $\mathfrak{g}(x) \geq \mathfrak{g}_0 > 0$ for all x. To stabilize the origin, a state-feedback control law is designed to constrain the motion of the system to the sliding manifold

$$s = \alpha_s x_1 + x_2 = 0. \tag{4.26}$$

On this manifold, the motion is governed by $\dot{x}_1 = -\alpha x_1$. Choosing $\alpha_s > 0$ guarantees that $x(t)$ tends to zero as t goes to infinity, and the rate of convergence can be controlled by choice of α. The motion on the manifold $s = 0$ is independent of $\mathfrak{h}$ and $\mathfrak{g}$. The variable s satisfies the equation

$$\dot{s} = \alpha_s \dot{x}_1 + \dot{x}_2 = \alpha_s x_2 + \mathfrak{h}(x) + \mathfrak{g}(x)u \tag{4.27}$$

Suppose $\mathfrak{h}$ and $\mathfrak{g}$ satisfy the inequality

$$\left| \frac{\alpha_s x_2 + \mathfrak{h}(x)}{\mathfrak{g}(x)} \right| \leq \varrho(x) \tag{4.28}$$

for some known function $\varrho(x)$. The stability of the sliding manifold is determined with the positive definite Lyapunov function candidate $\mathcal{V}(x) = \frac{1}{2}s^2$, where

$$\dot{\mathcal{V}} = s\dot{s} = s(\alpha x_2 + \mathfrak{h}(x)) + \mathfrak{g}(x)su \leq \mathfrak{g}(x)|s|\varrho(x) + \mathfrak{g}(x)su \tag{4.29}$$

Taking

$$u = -\beta_s(x)\text{sgn}(s) \tag{4.30}$$

where $\beta_s(x) \geq \varrho(x) + \beta_{s_0}$, $\beta_{s_0} > 0$, and

$$\text{sgn}(s) = \begin{cases} 1, & s > 0 \\ 0 & s = 0 \\ -1, & s < 0 \end{cases} \tag{4.31}$$

yields

$$\dot{\mathcal{V}} \leq \mathfrak{g}(x)|s|\varrho(x) - \mathfrak{g}(x)s(\varrho(x) + \beta_{s_0})\text{sgn}(s) = -\mathfrak{g}(x)\beta_{s_0}|s| \leq -\mathfrak{g}_0\beta_{s_0}|s| \tag{4.32}$$

Thus, $W = \sqrt{2\mathcal{V}} = |s|$ satisfies the differential inequality $\mathcal{D}^+ W \leq -\mathfrak{g}_0 \beta_{s_0}$, and the comparison lemma shows that $W(s(t)) \leq W(s(0)) - \mathfrak{g}_0 \beta_{s_0}$. Therefore, the trajectory reaches the manifold $s = 0$ in finite time and, once om the manifold, it cannot leave it, as seen from the inequality $\dot{\mathcal{V}} \leq -\mathfrak{g}_0 \beta_{s_0} |s|$. In summary, the motion consists of a reaching phase during which trajectories starting off the manifold $s = 0$ move toward it and reach it in finite time, followed by a sliding phase during which the motion is confined to the manifold $s = 0$ and the dynamics of the system are represented by the RO model $\dot{x}_1 = -\alpha_s x_1$. The manifold $s = 0$ is called the sliding manifold, and the control law $u = -\beta_s(x)\text{sgn}(s)$ is called the sliding mode control. The striking feature of sliding mode control is its robustness with respect to $\mathfrak{h}$ and $\mathfrak{g}$. We only need to know the upper bound $\varrho(x)$, and during the sliding phase, the motion is completely independent of $\mathfrak{h}$ and $\mathfrak{g}$. The sliding mode controller simplifies if $\mathfrak{h}$ and $\mathfrak{g}$ satisfy the inequality

$$\left| \frac{\alpha_s x_2 + \mathfrak{h}(x)}{\mathfrak{g}(x)} \right| \leq k_{SMC} \tag{4.33}$$

for some known nonnegative constant k_{SMC}. In this case, we can take

$$u = -K_{SMC}\text{sgn}(s), \quad K_{SMC} > k_{SMC} \tag{4.34}$$

which takes the form of a simple relay. This form, however, usually leads to a finite region of attraction, which can be estimated.

Because of imperfections in switching devices and delays, SMC suffers from chattering. As the trajectory heads towards $s = 0$, it hits the manifold at some point. Although it would ideally begin to slide along that manifold, delays between the time the sign of s changes and the time the control switches causes the trajectory to cross the manifold. When the control switches, the trajectory reverses directions and heads towards the manifold; however, it will cross the manifold again, repeating this process. Chattering can cause low control accuracy, high heat losses in electrical power circuits, and high wear of moving mechanical parts. It

may also excite unmodeled high-frequency dynamics, which degrades the performance of the system and may even lead to instability. This is especially possible for a rigid-flexible system that consists of a large range of frequencies [43].

In application of the CSMC to a rigid-flexible structure, consider Eq. (3.49). If the sliding manifold is defined as

$$s(t) = C_{CSMC}\epsilon + \dot{\epsilon} \tag{4.35}$$

where C_{CSMC} is a positive scalar constant, $\epsilon = x - x_d$ is the difference between the actual position states $x = [\theta, \bar{d}^T]^T$ and desired position states $x_d = [\theta_d, \bar{d}_d^T]^T$, and $\dot{\epsilon} = \dot{x} - \dot{x}_d$ is the difference between the actual velocity states and desired velocity states, the sliding surface will begin with a non-zero error for desired non-zero states. Unless a nonlinear surface with an initial zero error is defined, or the desired states are selected as functions of time that start at the initial conditions and go to the final desired states, the motion may not remain stable. Note that Eq. (3.49) does not include any matched uncertainties. Instead, some uncertainty in the model is included in Eq. (3.49) such that the equations of motion become

$$[M_I + \delta M]\ddot{x} + [D_I + \delta D]\dot{x} + [K_I + \delta K]x = [F](u_I + u_{SMC}) \tag{4.36}$$

where $M = M_I + \delta M$, $D = D_I + \delta D$, $K = K_I + \delta K$, and $u = u_I + u_{SMC}$. The actual mass, damping, and stiffness matrices are written as the sum of their ideal matrices (M_I, D_I, K_I) without uncertainties and model uncertainties $(\delta M, \delta D, \delta K)$. The total control input is also written as a sum of the nominal control u_I for an ideal system without uncertainties and control that mitigates the uncertainty u_{SMC}. The nominal control is computed by state feedback controllers, such as PID, LQR, and Lyapunov-based controllers to name a few. The uncertainty control is computed by the SMC law defined in Eq. (4.35); however, the state error terms e and $\dot{e}$ are defined differently. The error $\bar{e}$ is now the difference between the actual states of the system x and the ideal states x_I of the system without uncertainties.

The nominal control law and CSMC law, respectively, are defined as

$$u_I = -K_g x_I + r(t) \tag{4.37}$$

and

$$u_{CSMC} = -K_{CSMC}\text{sgn}(s) \tag{4.38}$$

where $K_{CSMC} \in \mathbb{R}^{1\times 2p}$ is the upper uncertainty bound. Because the sliding surface is no longer a function of the error between the current state and desired state that was non-zero at initial conditions but instead a function of the error between the actual state and ideal state, it is zero at initial conditions and maintains stable motion as the actual states try to remain equal to the ideal states, which are tracking the desired states. This also allows for the desired states to be chosen as constants if desired.

A prominent source of chattering from SMC can be found from the implementation of the sign function, $\text{sgn}(\cdot)$. As defined in Eq. (4.31), the sign function is an odd function, i.e. $\text{sgn}(-s) = -\text{sgn}(s)$, that returns the positive or negative sign of a real number. As the derivative of the absolute value function, up to but not including the indeterminacy at zero, the sign function provides a discontinuous step between -1 and 1 [45]. Although providing the full control effort instantaneously at each time t, the trajectory can never remain smoothly on the manifold because of this. One solution is to replace the sign function with an error function, $\text{erf}(\cdot)$. The error function is defined by the integral

$$\text{erf}(s) = \frac{2}{\sqrt{\pi}} \int_0^s \exp -t^2 \, \mathrm{d}t \tag{4.39}$$

This function is encountered in probability theory, the theory of errors, the theory of heat conduction, and various branches of mathematical physics [46]. By representing the exponential function in Eq. (4.39) in terms of its power series expansion, we have

$$\operatorname{erf}(s) = \frac{2}{\sqrt{\pi}} \int_0^s \sum_{n=0}^{\infty} \frac{(-1)^n}{n!} t^{2n} \, \mathrm{d}t \tag{4.40}$$

from which we deduce

$$\operatorname{erf}(s) = \frac{2}{\sqrt{\pi}} \sum_{n=0}^{\infty} \frac{(-1)^n s^{2n+1}}{n!(2n+1)} \quad |s| < \infty \tag{4.41}$$

Examination of Eq. (4.41) reveals that the error function is also an odd function. We also see that

$$\operatorname{erf}(0) = \frac{2}{\sqrt{\pi}} \int_0^0 \exp -t^2 \, \mathrm{d}t = 0 \tag{4.42}$$

and

$$\operatorname{erf}(\infty) = \frac{2}{\sqrt{\pi}} \int_0^\infty \exp -t^2 \, \mathrm{d}t = 1 \tag{4.43}$$

A graph of $\operatorname{erf}(s)$ is shown in Figure 4.1 to demonstrate this.

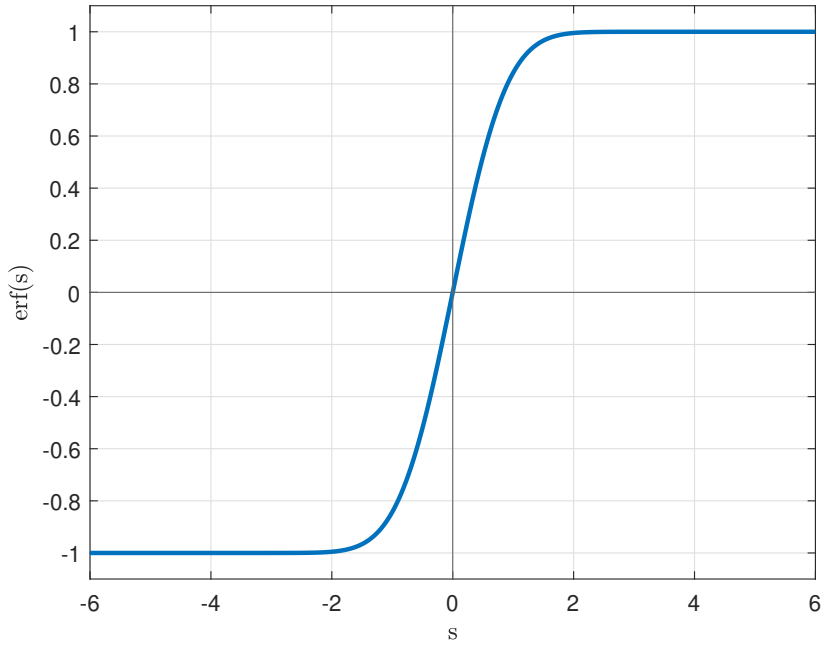

Figure 4.1 Relationship between error function $\operatorname{erf}(s)$ and s.

The important behavior of this function pertains to its final limits and convergence to known values at quantitative arguments. Unlike the sign function, the error function does not have a discontinuity between the negative and positive convergence values, which can reduce the chattering present in SMC. In return, the transition rate from -1 and 1 decreases, which may pose an issue if the system cannot acquire the necessary control input to achieve its desired control objectives and result in steady-state errors or even instability. A modified error function defined as

$$\operatorname{erf}\left(\frac{s}{\sqrt{2\sigma^2}}\right), \tag{4.44}$$

where σ is the standard deviation that stipulates how quickly the switch is activated, can be applied to provided further control tuning by manipulating the transition rate [47].

It is important to note that this combination of control laws from Eqs. (4.37) and (4.38) behaves similar to an observer-based control law. Instead of estimating the system's state to a true state, we are controlling the actual (true) state x to go to the ideal state x_I, which requires full knowledge of at least one of the systems. Because the actual system contains some arbitrary uncertainties in the model, all the states in the ideal system are assumed to be measurable, or known. This in turn determines the control gain of the ideal controller as well as to which system the observers are applied. Any FO and RO observers will be applied only to the actual system since no state estimation is needed for an ideal system in which all state variables are known.

Adaptive Sliding Mode Control

An alternative to CSMC is an adaptive smooth control scheme for robust control which attenuates chattering, eliminates the reaching phase, and successfully updates the control gain in real time [31]. A sliding manifold with no singularity is defined to improve the performance throughout the control implementation. Since the reaching phase vanishes, robustness against uncertainties and perturbations is guaranteed from the beginning. The

new sliding manifold has more flexibility to improve the transient performance in comparison with CSMC. Based on the concept of CSMC, a simple but robust controller in continuous fashion is also derived, and an adaptive gain-tuning algorithm is developed. The developed algorithm guarantees that the error converges to a small domain in a finite time without knowing the uncertainty bounds. Also, the gain update is performed using only the magnitude of the control input, which greatly eases the application of the suggested algorithm to real-world systems. This approach designed by Cho et al. [31] is applicable to stabilization and trajectory tracking. However, Cho et al. [31] designed the ASMC control law and adaptive rule for a problem in scalar dimensions, so the control law must be adapted to a vector-matrix form that requires a new stability analysis.

The sliding manifold $s(t) \in \mathbb{R}^g$ is defined as

$$s(t) = \dot{\epsilon}(t) + \Big(\Lambda + \mu\big(\exp(-\epsilon^T(t)\epsilon(t)) - 1\big)\Big)\epsilon(t) \tag{4.45}$$

where $s(t)$ is a directly related function of the system's states. Λ and μ are constants, in which $\Lambda > \mu > 0$. It should be noted that at the initial time $t = t_0$, if $\epsilon(t_0)$ and $\dot{\epsilon}(t_0)$ are zero, the sliding variable in Eq. (4.45) becomes zero, eliminating the reaching phase. Also, by properly selecting the parameters Λ and μ, one can improve the transient response more flexibly than when using a CSMC.

Consider an uncertain system with the sliding variable feedback control [31]

$$u_{ASMC}(t) = -\frac{1}{\varepsilon}K^T_{ASMC}(t)s(t) \tag{4.46}$$

where ε is a small positive scalar number. If $||s(t_0)|| > \varepsilon$, then the state trajectories converge to the region $||s(t)|| \leq \varepsilon$ in a finite time and remain in the region thereafter. The time-varying gain matrix $K_{ASMC}(t) \in \mathbb{R}^{g\times r}$, for $(g \geq r)$ only, is constructed in the following manner. $K_{ASMC}(t)$ is a matrix of ones and zeros and multiplied by a time-varying scalar gain $\kappa_g(t)$. The gain $\kappa_g(t)$ has an upper bound, i.e., there exists a positive constant κ^*_g such

that $\kappa_g \leq \kappa_g^*$ for all $t \geq 0$. The location of every 1 is determined by the number of control inputs r and the listed order of each control input in the control input vector $u(t)$. All other remaining matrix elements are filled with zeros. For example, if the control input is defined as $u(t) = [u_1(t),\ u_2(t)]^T$, the gain matrix must be organized as

$$K_{ASMC}(t) = \kappa_g(t) \begin{bmatrix} 1 & 0 \\ 0 & 1 \\ 0 & 0 \\ \vdots & \vdots \\ 0 & 0 \end{bmatrix}$$

$K_{ASMC}(t)$ is constructed in this fashion for several reasons. This allows the adaptive rule for $\kappa_g(t)$ to remain scalar, applying the time-varying gain equally to each sliding surface element that requires control and simplifying the stability analysis of ASMC.

Suppose that one can represent the highest time-order derivative of the system output in the form

$$Y^{(\bar{n})}(X,t) = \xi_A(X,t) + b_A(X,t)u(t) \tag{4.47}$$

where $\bar{n}$ is the highest order of differentiation of the system states, and $\xi_A(X,t) \in \mathbb{R}^g$ and $b_A(X,t) \in \mathbb{R}^{g\times r} \neq 0$ are unknown. It is important to note that applying a similarity transformation to convert the system states to modal coordinates is necessary to acquire a $b_A(X,t)$ that will provide non-negative definiteness when multiplied to with $K_{ASMC}^T(t)$ later in the stability analysis. This is acquired by solving the eigenvalue problem for an undamped system, i.e., $(K - \omega_n^2 M)\bar{\Psi} = \bar{0}$, where $\bar{\Psi} \in \mathbb{R}^p$ is the eigenvector. By using Eq. (4.45), its differentiation with respect to time yields

$$
\begin{aligned}
\dot{s}(t) &= \ddot{\epsilon}(t) + \Big(\Lambda + \mu\big(\exp(-\epsilon^T(t)\epsilon(t)) - 1\big)\Big)\dot{\epsilon}(t) \\
&\quad + \Big(- 2\mu\epsilon^T(t)\dot{\epsilon}(t)\exp(-\epsilon^T(t)\epsilon(t))\Big)\epsilon(t) \\
&= \ddot{y}(t) - \ddot{y}_d(t) + \Big(\Lambda + \mu\big(\exp(-\epsilon^T(t)\epsilon(t)) - 1\big)\Big)\dot{\epsilon}(t) \\
&\quad + \Big(- 2\mu\epsilon^T(t)\dot{\epsilon}(t)\exp(-\epsilon^T(t)\epsilon(t))\Big)\epsilon(t) \\
&= \xi_A(X,t) - \ddot{y}_d(t) + \Big(\Lambda + \mu\big(\exp(-\epsilon^T(t)\epsilon(t))\dot{\epsilon}(t) - 1\big)\Big)\dot{\epsilon}(t) \\
&\quad + \Big(- 2\mu\epsilon^T(t)\dot{\epsilon}(t)\exp(-\epsilon^T(t)\epsilon(t))\Big)\epsilon(t) + b_A(X,t)u(t) \\
&\triangleq z(X,t) + b_A(X,t)u(t)
\end{aligned}
\tag{4.48}
$$

where $z(X,t) \in \mathbb{R}^{g\times 1}$ and $b_A(X,t)$ are functions bounded by

$$
||z(X,t)|| < \Gamma_r,\ 0 < b_r < ||b_A(X,t)|| < B_r \tag{4.49}
$$

and the uncertainty bounds Γ_r, b_r, and B_r are assumed to exist but are unknown. Note that all norms applied are Frobenius norms, which are equivalent to 2-norms for the case of all single-column vectors. Although the boundedness condition Eq. (4.49) is a common assumption in SMC literature, it guarantees only local or semi-global stability results since one cannot state that the uncertainty is globally uniformly bounded by some constant on the overall domain. Instead, Eq. (4.49) is used to simplify the presentation since we are interested in applying adaptation laws to counteract the unknown bounds. We do not, therefore, assume variable bounds with *known* upper bounds, as usually carried out in the absence of adaptive control laws [31].

Cho et al. [31] first considered a sliding variable feedback control with the time-varying gain $\kappa_R(t)$ instead of $\kappa_g(t)$, where $\kappa_R(t)$ is a continuous function of time and $\kappa_R(t) \geq \kappa_r \triangleq \frac{\Gamma_r}{b_r}$ is satisfied for the time $t \geq t_0$. However, as determined by Cho et al. [31], the maximum magnitude if the control input will be equal to the unknown real gain $\kappa_r = \frac{\Gamma_r}{b_r}$ only when

$s(t)$ is eventually bounded by the region $||s(t)|| \leq \hat{\varepsilon}$, where $\hat{\varepsilon}$ is the upper bound on $||s(t)||$ for an estimated constant gain $\hat{\kappa}_g$. Thus, an adaptive rule is necessary to obtain the gain.

The time-varying gain $\kappa_g(t)$ is updated in real time by the adaptive law

$$\dot{\kappa}_g(t) = \eta(||u_{ASMC}|| - \kappa_g(t) + \kappa_{g_0}), \quad \kappa_g(0) \geq \kappa_{g_0} \tag{4.50}$$

where κ_{g_0} and η are specified positive constants. The control law $u_{ASMC}(t)$ is given by Eq. (4.46), and κ_{g_0} is reserved for margin. As soon as the gain $\kappa_g(t)$ becomes greater than a specific value $(\kappa_r + \kappa_{g_0})$ at the time instant $t = t_0$, $||s(t)||$ decreases and there exists a finite time $t_1 > t_0$ before which $\kappa_g(t)$ becomes smaller than $(\kappa_r + \kappa_{g_0})$. Furthermore, during this finite-time interval, $\kappa_g(t)$'s upper bound $\kappa_g^* < \infty$ can be explicitly obtained. When the gain becomes greater than $(\kappa_r + \kappa_{g_0})$, the process restarts.

Before proceeding with the stability analysis of the ASMC, however, one final assumption is made. It is assumed that only the system states that are controllable are considered. The total number of controllable states is denoted by g'. Therefore, the sliding manifold $s(t)$ becomes $s'(t) \in \mathbb{R}^{g'}$, a function of $\epsilon'(t)$ and $\dot{\epsilon}'(t)$, which are the errors of the controllable states. Following suit, $\xi_A(X,t)$, $z(X,t)$, $b_A(X,t)$, $Y^{(\bar{n})}(X,t)$, and $K_{ASMC}(t)$ are rewritten as $\xi'_A(X,t) \in \mathbb{R}^{g'}$, $z'(X,t) \in \mathbb{R}^{g'}$, $b'_A(X,t) \in \mathbb{R}^{g' \times r}$, $Y'^{(\bar{n})}(X,t) \in \mathbb{R}^{g'}$, and $K'_{ASMC}(t) \in \mathbb{R}^{g' \times r}$ respectively. The uncertainty bounds for $z'(X,t)$ and $b'_A(X,t)$ are still valid after this assumption since $||z'(X,t)|| < ||z(X,t)|| < \Gamma_r$ and $0 < b'_r < ||b'(X,t)|| < ||b(X,t)|| < B_r$. This assumption will be referred to as the g' assumption and is necessary in order to ensure that the number of control inputs is equal to the number of controllable output states ($r = g'$), which will become an important consideration in the stability analysis later on.

The stability of the ASMC is analyzed with the Lyapunov candidate function

$$\mathcal{V}_A = \frac{1}{2} s'^T s' + \frac{1}{2\gamma_A}(\kappa_g - \kappa_g^*)^2 \tag{4.51}$$

where γ_A is a positive scalar constant. Taking the first order derivative of Eq. (4.51) with

respect to time and substituting $\dot{s}$ using Eq. (4.48) yields

$$\begin{aligned}\dot{\mathcal{V}}_A &= s'^T\dot{s}' + \frac{1}{\gamma_A}(\kappa_g - \kappa_g^*)\dot{\kappa}_g \\ &= s'^T(z' + b'_A u) + \frac{1}{\gamma_A}(\kappa_g - \kappa_g^*)\dot{\kappa}_g \\ &= s'^T\left(z' - \frac{1}{\varepsilon}b'_A K'^T_{ASMC}s'\right) + \frac{1}{\gamma_A}(\kappa_g - \kappa_g^*)\dot{\kappa}_g\end{aligned} \tag{4.52}$$

In order to utilize the matrix property $\lambda_{min}(W)||x||^2 \leq x^T W x \leq \lambda_{max}(W)||x||^2$, the matrix W must be a symmetric matrix that guarantees $x^T W x$ to be non-negative. The matrix $b'_A K'^T_{ASMC}$ can be rewritten as the sum of its skew-symmetric and symmetric components, i.e., $b'_A K'^T_{ASMC} = \frac{1}{2}\left(b'_A K'^T_{ASMC} - (b'_A K'^T_{ASMC})^T\right) + \frac{1}{2}\left(b'_A K'^T_{ASMC} + (b'_A K'^T_{ASMC})^T\right)$. In this form, $s'^T\left(\frac{1}{2}\left(b'_A K'^T_{ASMC} - (b'_A K'^T_{ASMC})^T\right)\right)s' = 0$, so only the symmetric component remains. By substituting the symmetric component for W and utilizing $\lambda_{min}\left(\frac{1}{2}\left(b'_A K'^T_{ASMC} + (b'_A K'^T_{ASMC})^T\right)\right)||s'||^2$, $\dot{\mathcal{V}}_A$ becomes

$$\begin{aligned}\dot{\mathcal{V}}_A &= s'^T\left(z' - \frac{1}{\varepsilon}\left(\frac{1}{2}\left(b'_A K'^T_{ASMC} + (b'_A K'^T_{ASMC})^T\right)\right)s'\right) + \frac{1}{\gamma_A}(\kappa_g - \kappa_g^*)\dot{\kappa}_g \\ &< ||s'||\left(\Gamma_r - \frac{1}{\varepsilon}\lambda_{min}\left(\frac{1}{2}\left(b'_A K'^T_{ASMC} + (b'_A K'^T_{ASMC})^T\right)\right)||s'||\right) + \frac{1}{\gamma_A}(\kappa_g - \kappa_g^*)\dot{\kappa}_g\end{aligned} \tag{4.53}$$

The case when $||s'(t)|| > \varepsilon'$ is considered. Using some algebraic manipulation and the definition of κ_r, $\dot{\mathcal{V}}$ becomes

$$
\begin{aligned}
\dot{\mathcal{V}}_A &< ||s'||\left(\Gamma_r - \frac{1}{\varepsilon}\lambda_{min}\left(\frac{1}{2}\left(b'_A K'^T_{ASMC} + (b'_A K'^T_{ASMC})^T\right)\right)||s'||\right) + \frac{1}{\gamma_A}(\kappa_g - \kappa_g^*)\dot{\kappa}_g \\
&= ||s'||\left(\Gamma_r - \frac{1}{\varepsilon}\lambda_{min}\left(\frac{1}{2}\left(b'_A K'^T_{ASMC} + (b'_A K'^T_{ASMC})^T\right)\right)||s'||\right) + \frac{1}{\gamma_A}(\kappa_g - \kappa_g^*)\dot{\kappa}_g \\
&\quad + ||s'||||b'_A||\kappa_g^* - ||s'||||b'_A||\kappa_g^* \\
&< ||s'||\left(\Gamma_r - ||b'_A||\kappa_g^*\right) + \frac{1}{\gamma_A}(\kappa_g - \kappa_g^*)\dot{\kappa}_g + ||s'||||b'_A||\kappa_g^* \\
&\quad - \frac{1}{\varepsilon}||s'||\lambda_{min}\left(\frac{1}{2}\left(b'_A K'^T_{ASMC} + (b'_A K'^T_{ASMC})^T\right)\right) \\
&= ||s'||\left(b'_r\kappa_r - ||b'_A||\kappa_g^*\right) - \frac{1}{\gamma_A}|\kappa_g - \kappa_g^*|\dot{\kappa}_g + ||s'||||b'_A||\kappa_g^* \\
&\quad - \frac{1}{\varepsilon}||s'||\lambda_{min}\left(\frac{1}{2}\left(b'_A K'^T_{ASMC} + (b'_A K'^T_{ASMC})^T\right)\right)
\end{aligned}
\tag{4.54}
$$

where $b'_r\kappa_r - ||b'_A||\kappa_g^* < 0$, $(\kappa_g - \kappa_g^*) = -|\kappa_g - \kappa_g^*|$, and a proper selection of γ_A will always make

$$
-\frac{1}{\gamma_A}|\kappa_g - \kappa_g^*|\dot{\kappa}_g + ||s'||||b'_A||\kappa_g^* - ||s'||\lambda_{min}\left(\frac{1}{2}\left(b'_A K'^T_{ASMC} + (b'_A K'^T_{ASMC})^T\right)\right) < 0
$$

This condition yields

$$
\gamma_A < \frac{|\kappa_g - \kappa_g^*|\dot{\kappa}_g}{||s'||\lambda_{min}\left(\frac{1}{2}\left(b'_A K'^T_{ASMC} + (b'_A K'^T_{ASMC})^T\right)\right) - ||s'||||b'_A||\kappa_g^*}
\tag{4.55}
$$

Substituting Eq. (4.50) into Eq. (4.55) yields

$$\begin{aligned}\gamma_A &< \frac{|\kappa_g - \kappa_g^*|\eta(||u_{ASMC}|| - \kappa_g(t) + \kappa_{g_0})}{||s'||\lambda_{min}\left(\frac{1}{2}\left(b'_A K'^T_{ASMC} + (b'_A K'^T_{ASMC})^T\right)\right) - ||s'||||b'_A||\kappa_g^*} \\ &= \frac{|\kappa_g - \kappa_g^*|\eta(\frac{1}{\varepsilon}||K'^T_{ASMC}s'|| - \kappa_g(t) + \kappa_{g_0})}{||s'||\lambda_{min}\left(\frac{1}{2}\left(b'_A K'^T_{ASMC} + (b'_A K'^T_{ASMC})^T\right)\right) - ||s'||||b'_A||\kappa_g^*}\end{aligned} \tag{4.56}$$

One can select γ_A so that it is less than the minimum of the right-hand side of Eq. (4.56). Let $\Theta(t)$ be defined as

$$\Theta(t) \triangleq \frac{|\kappa_g - \kappa_g^*|\eta(\frac{1}{\varepsilon}||K'^T_{ASMC}s'|| - \kappa_g(t) + \kappa_{g_0})}{||s'||\lambda_{min}\left(\frac{1}{2}\left(b'_A K'^T_{ASMC} + (b'_A K'^T_{ASMC})^T\right)\right) - ||s'||||b'_A||\kappa_g^*} \tag{4.57}$$

Note that the case $||s'(t)|| > \varepsilon'$ is being considered, and $\kappa_g(t)$ is always greater than κ_{g_0}. Then, the numerator and denominator of $\Theta(t)$ are positive, so

$$\begin{aligned}\Theta(t) &> \frac{|\kappa_g - \kappa_g^*|\eta(\frac{1}{\varepsilon}||K'^T_{ASMC}s'|| - \kappa_g(t) + \kappa_{g_0})}{||s'||||b'_A||\kappa_g - ||s'||||b'_A||\kappa_g^*} \\ &= \frac{|\kappa_g - \kappa_g^*|\eta(\frac{1}{\varepsilon}||K'^T_{ASMC}s'|| - \kappa_g(t) + \kappa_{g_0})}{||s'||||b'_A|||\kappa_g - \kappa_g^*|} \\ &= \frac{\eta(\frac{1}{\varepsilon}||K'^T_{ASMC}s'|| - \kappa_g(t) + \kappa_{g_0})}{||s'||||b'_A||}\end{aligned} \tag{4.58}$$

where $\lambda_{min}\left(\frac{1}{2}\left(b'_A K'^T_{ASMC} + (b'_A K'^T_{ASMC})^T\right)\right) < ||b'_A||\kappa_g$. The right-hand side of Eq. (4.58) has its minimum when $\kappa_g(t) = \kappa_{g_0}$ such that

$$\Theta(t) > \frac{\eta(\frac{1}{\varepsilon}||K'^T_{ASMC}s'|| - \kappa_g(t) + \kappa_{g_0})}{||s'||||b'_A||} \geq \frac{\eta(\frac{1}{\varepsilon}||K'^T_{ASMC_0}s'||)}{||s'||||b'_A||} \tag{4.59}$$

where K'_{ASMC_0} is obtained by replacing $\kappa_g(t)$ with κ_{g_0} in K'_{ASMC}. Furthermore,

$$\frac{\eta(\frac{1}{\varepsilon}||K'^T_{ASMC_0}s'||)}{||s'||||b'_A||} > \frac{\eta(\frac{1}{\varepsilon}||K'^T_{ASMC_0}s'||)}{||s'||B_r} \tag{4.60}$$

since $||b'_A|| < B_r$. Lastly, recall the g' assumption made before the stability analysis. $||K^T_{ASMC_0}s||$ can be rewritten as $\kappa_{g_0}\sqrt{\sum_{j=1}^{m}|s_j|^2}$, and $\kappa_{g_0}||s||$ is defined as $\kappa_{g_0}\sqrt{\sum_{j=1}^{g}|s_j|^2}$. Without this assumption, the number of output states is less than or equal to the number of control inputs, i.e., $r \leq g$. This inequality is directly related to the inequality between $||K^T_{ASMC_0}s||$ and $\kappa_{g_0}||s||$, i.e., $||K^T_{ASMC_0}s|| \leq \kappa_{g_0}||s||$. Substitution of $||K^T_{ASMC_0}s||$ with $\kappa_{g_0}||s||$ would violate the minimization of γ_A whenever $r < g$. Therefore, the g' assumption is made to ensure that the number of control inputs is always equal to the number of controllable output states, i.e., $r = g'$ and $||K'^T_{ASMC_0}s'|| = \kappa_{g_0}||s'||$. Substituting $||K'^T_{ASMC_0}s'|| = \kappa_{g_0}||s'||$ into the right-hand side of Eq. (4.60) further minimizes the equation, i.e.,

$$\begin{aligned}\frac{\eta(\frac{1}{\varepsilon}||K'^T_{ASMC_0}s'||)}{||s'||B_r} &> \frac{\eta(\frac{1}{\varepsilon}\kappa_{g_0}||s'||)}{||s'||B_r} \\ &= \frac{\eta\kappa_{g_0}}{\varepsilon B_r}\end{aligned} \tag{4.61}$$

Therefore, one can select γ_A such that

$$\gamma_A < \frac{\eta\kappa_{g_0}}{\varepsilon B_r} \tag{4.62}$$

and the finite-time convergence to the region $||s(t)|| \leq \varepsilon$ is guaranteed from the moment when $||s(t)|| > \varepsilon$ starts to hold.

4.4 State Estimation for Feedback Control

In many systems all components of the state vector are not directly available as output signals. As previously mentioned in the last section, the reason for wanting knowledge of the states is for forming feedback control signals. Several approaches to this problem can be considered. The first, and most direct, way is to simply add additional sensors that can provide measurements for all the state variables, but this method is generally expensive or unfeasible. A second option involves differentiation of the measured states that may provide an estimate of the unmeasured states. However, differentiation may not give sufficiently

accurate performance, especially since any noise in the data will also be propagated and become noisier. A third approach that is most commonly used is to utilize the full knowledge of the mathematical models of the system in a systematic way in an attempt to estimate, or reconstruct, the states. This resulting algorithm is called a state estimator, or observer. Along with state estimation, an observer is designed with the objective to achieve suitable pole locations for these estimated model states that will maintain a stable system and produce desired performance.

4.4.1 Full-Order Observer-Based Feedback Control

FO observers produce estimates of all state variables, both measurable and unmeasurable. Along with full-state estimation, FO observers also provide a smoothing effect when measurements are noisy. Consider the observer system model

$$\dot{\hat{X}}(t) = A\hat{X}(t) + Bu(t) + L_{g_{FO}}(Y(t) - \hat{Y}(t)) \tag{4.63a}$$

$$\hat{Y}(t) = C\hat{X}(t) \tag{4.63b}$$

where $\hat{X}(t)$ is the augmented state estimate vector, $\hat{Y}(t)$ is the estimated output vector, and $L_{g_{FO}}$ is the constant FO observer gain matrix. An estimation error between the true state variables and estimates is defined as

$$\epsilon_{FO}(t) = X(t) - \hat{X}(t) \tag{4.64}$$

By taking the first-order time-derivative of Eq. (4.64) and using Eqs. (4.1a) and (4.63a), the error dynamics are obtained as

$$\begin{aligned}\dot{\epsilon}_{FO}(t) &= \dot{X}(t) - \dot{\hat{X}}(t) \\ &= AX(t) + Bu - (A\hat{X}(t) + Bu + L_{g_{FO}}(Y(t) - \hat{Y}(t))) \\ &= A(X(t) - \hat{X}(t)) - L_{g_{FO}}C(X(t) - \hat{X}(t)) \\ &= (A - L_{g_{FO}}C)\epsilon_{FO}(t)\end{aligned} \tag{4.65}$$

with initial conditions $\epsilon_{FO}(0) = X(0) - \hat{X}(0)$. Note that the initial conditions of the estimated states are not necessarily the same as the initial conditions of the true states. The observer is then designed such that it provides an asymptotically convergent estimate of the states. This is done by obtaining an constant FO observer gain matrix $L_{g_{FO}}$ such that $A - L_{g_{FO}}C$ yields the desired eigenvalues. In fact, there is a duality between obtaining the constant state-feedback gain matrix K_g and the observer gain matrix. By including the observer in the system model, the state variables are replaced with the state estimates in the control input, and the system control law becomes

$$u(t) = -K_g\hat{X} + r(t) \tag{4.66}$$

where $r(t)$ is some reference input for tracking a desired state. The new linear closed-loop system that includes the FO observer-based feedback control can be written as

$$\begin{bmatrix} \dot{X}(t) \\ \dot{\epsilon}_{FO}(t) \end{bmatrix} = \begin{bmatrix} A - BK_g & BK_g \\ 0_{2p\times 2p} & A - L_{g_{FO}}C \end{bmatrix} \begin{bmatrix} X(t) \\ \epsilon_{FO}(t) \end{bmatrix} + \begin{bmatrix} B \\ 0_{2p\times 1} \end{bmatrix} r(t) \tag{4.67}$$

If the augmented state vector is chosen to be $[X^T(t)\ \hat{X}_{FO}^T(t)]^T$, the closed-loop system can be written as

$$\begin{bmatrix} \dot{X}(t) \\ \dot{\hat{X}}_{FO}(t) \end{bmatrix} = \begin{bmatrix} A & -BK_g \\ L_{g_{FO}}C & A - BK_g - L_{g_{FO}}C \end{bmatrix} \begin{bmatrix} X(t) \\ \hat{X}_{FO}(t) \end{bmatrix} + \begin{bmatrix} B \\ B \end{bmatrix} r(t) \tag{4.68}$$

The two augmented state vectors above are related by the invertible mapping

$$\begin{bmatrix} X(t) \\ \epsilon_{FO}(t) \end{bmatrix} = \begin{bmatrix} I_{2p} & \bar{0}_{2p\times 2p} \\ I_{2p} & -I_{2p} \end{bmatrix} \begin{bmatrix} X(t) \\ \hat{X}_{FO}(t) \end{bmatrix} \tag{4.69}$$

One of the major uses of the state estimation observers is state feedback control system design. The observers described are used to estimate the state variables X. If a constant-state feedback matrix K_g is then used with $\hat{X}$ as input instead of X, a new composite system of the order $2(2p)$ is obtained. By proper selection of K_g, some of the $2p$ closed-loop eigenvalues can be specified. By proper selection of $L_{g_{FO}}$, the remaining eigenvalues of the observer can be specified. This represents the separation principle. If a feedback system with desired poles can be designed, proceeding as if all states were measurable, then a separate design of the observer can be used to provide the desired observer poles [40].

4.4.2 Reduced-Order Observer-Based Feedback Control

Utilization of a FO observer results in a redundancy when providing estimates for states that can already be measured. This redundancy can be avoided with a RO observer, which estimates only the states that are not measured and uses raw measurement data for those that are measured. Before considering an observer system, a transformation is defined such that s outputs constitute the first s states, perhaps modified by a Du term. The similarity transformation is defined as

$$Z(t) = TX(t) \tag{4.70}$$

where $T = [C^T, \mathcal{R}^T]^{-T} \in \mathbb{R}^{2p\times 2p}$, and $\mathcal{R} \in \mathbb{R}^{(2p-s)\times 2p}$ is obtained by solving $\mathcal{R}C^T = 0_{(2p-s)\times s}$ and $\mathcal{R}\mathcal{R}^T = I_{2p-s}$. One way to obtain $\mathcal{R}$ is by taking the transpose of the null space of C, or using the MATLAB function `null(C)'`. However, $\mathcal{R}$ can be any matrix such that T is invertible. Once the similarity transformation is obtained and applied to Eqs. (4.1a) and (4.1b), the state-space description of the transformed system becomes

$$\dot{Z}(t) = \tilde{A}Z(t) + \tilde{B}u(t) \tag{4.71a}$$

$$\tilde{Y}(t) = \tilde{C}Z(t) + Du(t) \tag{4.71b}$$

where $\tilde{A} = T^{-1}AT$, $\tilde{B} = T^{-1}B$, and $\tilde{C} = CT = [I_s \; 0_{s\times(2p-s)}]$. By designing an estimator for $Z(t) = [Z_1^T(t), Z_2^T(t)]^T \in \mathbb{R}^{2p}$, where $Z_1(t) \in \mathbb{R}^s$ and $Z_2(t) \in \mathbb{R}^{2p-s}$, that same estimator can be applied for $Z(t) = TX(t)$. The transformed system in Eqs. (4.71a) and (4.71b) can be written as

$$\begin{bmatrix} \dot{Z}_1(t) \\ \dot{Z}_2(t) \end{bmatrix} = \begin{bmatrix} \tilde{A}_{11} & \tilde{A}_{12} \\ \tilde{A}_{21} & \tilde{A}_{22} \end{bmatrix} \begin{bmatrix} Z_1(t) \\ Z_2(t) \end{bmatrix} + \begin{bmatrix} \tilde{B}_1 \\ \tilde{B}_2 \end{bmatrix} u(t) \tag{4.72a}$$

$$\tilde{Y}(t) = Z_1(t) + Du(t) \tag{4.72b}$$

where $\tilde{A}_{11} \in \mathbb{R}^{s\times s}$, $\tilde{A}_{12} \in \mathbb{R}^{s\times(2p-s)}$, $\tilde{A}_{21} \in \mathbb{R}^{(2p-s)\times s}$, $\tilde{A}_{22} \in \mathbb{R}^{(2p-s)\times(2p-s)}$, $\tilde{B}_1 \in \mathbb{R}^{s\times 1}$, and $\tilde{B}_2 \in \mathbb{R}^{(2p-s)\times 1}$. Since $Z_1(t)$ is already known, only $Z_2(t)$ requires an estimator. Hence, the state equations for $Z_2(t)$ are

$$\dot{Z}_2(t) = \tilde{A}_{22}Z_2(t) + \tilde{A}_{21}(\hat{Y}(t) - Du(t)) + \tilde{B}_2u(t) \tag{4.73}$$

In order to design an estimator for $Z_2(t)$, an output equation for $Z_2(t)$ is needed. The equation for $Z_1(t)$ in Eqs. (4.72a) and (4.72b) is used to solve for $\tilde{A}_{12}Z_2(t)$:

$$\begin{aligned}\tilde{A}_{12}Z_2(t) &= \dot{Z}_1(t) - \tilde{A}_{11}Z_1(t) - \tilde{B}_1u(t) \\ &= \dot{\tilde{Y}}(t) - \tilde{A}_{11}(\tilde{Y}(t) - Du(t)) - \tilde{B}_1u(t) - D\dot{u}(t)\end{aligned} \tag{4.74}$$

where $\dot{u}(t)$ is a smooth, first-order differentiation with respect to time of the control input, and $\tilde{A}_{12}Z_2(t)$ can then be set equal to some $\tilde{Y}_r(t)$ so that

$$\tilde{Y}_r(t) := \tilde{A}_{12}Z_2(t) = \dot{\tilde{Y}}(t) - \tilde{A}_{11}(\tilde{Y}(t) - Du(t)) - \tilde{B}_1u(t) - D\dot{u}(t) \tag{4.75}$$

Analogous to the FO observer design in Eq. (4.63a), and using the dynamics of the RO system in Eqs. (4.73) and (4.75), the $(2p-s)$-dimensional dynamic system of the RO observer is defined as

$$\begin{aligned}\dot{\hat{Z}}_2(t) =& \tilde{A}_{22}\hat{Z}_2(t) + \tilde{A}_{21}(\tilde{Y}(t) - Du(t)) + \tilde{B}_2u(t) + L_{g_{RO}}(\tilde{Y}_r(t) - \hat{Y}_r(t)) \\ =& \tilde{A}_{22}\hat{Z}_2(t) + \tilde{A}_{21}(\tilde{Y}(t) - Du(t)) + \tilde{B}_2u(t) + L_{g_{RO}}(\tilde{Y}_r(t) - \tilde{A}_{12}\hat{Z}_2(t))\end{aligned} \tag{4.76}$$

where $L_{g_{RO}}$ is the constant RO observer gain matrix. According to Eq. (4.75), the term $\tilde{Y}_r(t)$ in Eq. (4.76) includes the time derivative of the output, i.e. $\dot{\tilde{Y}}(t)$, which is generally not available for measurement. Furthermore, differentiating $\tilde{Y}(t)$ with respect to time is generally undesirable because of the undesirable noise amplification of a differentiator. In order to avoid differentiating the outputs, a new variable $\hat{\xi}(t)$ is defined as

$$\hat{\xi}(t) = \hat{Z}_2(t) - L_{g_{RO}}\tilde{Y}(t) \tag{4.77}$$

Differentiating both sides of Eq. (4.77) with respect to time and using Eqs. (4.75) and (4.76) yields

$$
\begin{aligned}
\dot{\hat{\xi}}(t) =& \dot{\hat{Z}}_2(t) - L_{g_{RO}}\dot{\tilde{Y}}(t) \\
=& (\tilde{A}_{22} - L_{g_{RO}}\tilde{A}_{12})\hat{\xi}(t) + (\tilde{A}_{22}L_{g_{RO}} - L_{g_{RO}}\tilde{A}_{12}L_{g_{RO}} + \tilde{A}_{21} - L_{g_{RO}}\tilde{A}_{11})\tilde{Y}(t) \\
&+ (\tilde{B}_2 - L_{g_{RO}}\tilde{B}_1 - \tilde{A}_{21}D + L_{g_{RO}}\tilde{A}_{11}D)u(t) - L_{g_{RO}}D\dot{u}(t)
\end{aligned} \tag{4.78}
$$

Recall that Eqs. (4.71a) and (4.71b) are obtained from Eqs. (4.1a) and (4.1b) using the similarity transformation. Hence, if (A, C) in (4.1a) and (4.1b) is an observable pair, then so is $(\tilde{A}, \tilde{C})$ in Eqs. (4.71a) and (4.71b). Furthermore, if $(\tilde{A}, \tilde{C})$ is an observable pair, then so is $(\tilde{A}_{22}, \tilde{A}_{12})$ in the RO system described by Eqs. (4.73) and (4.75). Therefore, an observer gain $L_{g_{RO}}$ can be designed. For the RO system, the estimation error is defined as

$$
\epsilon_{RO}(t) = Z_2(t) - \hat{Z}_2(t) \tag{4.79}
$$

After taking the first-order time-derivative of Eq. (4.79) and applying some algebra in a similar fashion as in Eq. (4.65), the error dynamics are obtained as

$$
\begin{aligned}
\dot{\epsilon}_{RO}(t) &= \dot{Z}_2(t) - \dot{\hat{Z}}_2(t) \\
&= (\tilde{A}_{22} - L_{g_{RO}}\tilde{A}_{12})\epsilon_{RO}(t)
\end{aligned} \tag{4.80}
$$

with initial conditions $\epsilon_{RO}(0) = Z_2(0) - \hat{Z}_2(0)$. In similar principle as the FO observer, the reduce-order observer gain matrix $L_{g_{RO}}$ is obtained such that $\tilde{A}_{22} - L_{g_{RO}}\tilde{A}_{12}$ yields desired eigenvalues that provide an asymptotically convergent estimate of $Z_2(t)$. The new linear close-loop system that includes the RO observer-based feedback control can be written as

$$
\begin{bmatrix} \dot{X}(t) \\ \dot{\epsilon}_{RO}(t) \end{bmatrix} = \begin{bmatrix} A - BK_g & BKT_2 \\ 0_{(2p-s)\times 2p} & \tilde{A}_{22} - L_{g_{RO}}\tilde{A}_{12} \end{bmatrix} \begin{bmatrix} X(t) \\ \epsilon_{RO}(t) \end{bmatrix} + \begin{bmatrix} B \\ 0_{(2p-s)\times 1} \end{bmatrix} r(t) \tag{4.81}
$$

where $T_1 \in \mathbb{R}^{2p\times s}$ and $T_2 \in \mathbb{R}^{2p\times(2p-s)}$ are partitions of $T = [T_1 \vdots T_2] \in \mathbb{R}^{2p\times 2p}$. If the

augmented state vector $[X^T(t)\ \hat{\xi}(t)]$ is used instead, the closed-loop system can be written as

$$\begin{bmatrix} \dot{X}(t) \\ \dot{\hat{\xi}}(t) \end{bmatrix} = \begin{bmatrix} \Xi_{11} & \Xi_{12} \\ \Xi_{21} & \Xi_{22} \end{bmatrix} \begin{bmatrix} X(t) \\ \hat{\xi}(t) \end{bmatrix} + \begin{bmatrix} B \\ \tilde{B}_2 - L_{g_{RO}}\tilde{B}_1 \end{bmatrix} r(t) \tag{4.82}$$

where $\Xi_{11} = A - BK_g(T_1 + T_2L_{g_{RO}})C$, $\Xi_{12} = -BK_gT_2$, $\Xi_{21} = -(\tilde{B}_2 - L_{g_{RO}}\tilde{B}_1)K_g(T_1 + T_2L_{g_{RO}})C$, and $\Xi_{22} = (\tilde{A}_{22} - L_{g_{RO}}\tilde{A}_{12}) - (\tilde{B}_2 - L_{g_{RO}}\tilde{B}_1)K_gT_2$. The inverse mapping between the two augmented state vectors is given as

$$\begin{bmatrix} X(t) \\ \epsilon_{RO}(t) \end{bmatrix} = \begin{bmatrix} I_{2p} & \bar{0}_{p\times p} \\ \mathcal{R} - L_{g_{RO}}C & -I_p \end{bmatrix} \begin{bmatrix} X(t) \\ \hat{\xi}(t) \end{bmatrix} \tag{4.83}$$

Similar to the FO observer-based feedback control, the separation principle also holds for the RO observer-based feedback control.

5 Numerical Simulations and Discussions

In this chapter, numerical simulations are presented for the formulated rigid-flexible body dynamics and designed control laws and state estimators. The physical parameters of the rigid-flexible system modeled in Figure 2.3 are listed in Table 5.1.

Table 5.1 Physical Parameters of the Rigid-Flexible System

Aluminum Beam	
L	1.7706 m
A	1.1089×10^{-4} m^2
ρ	2780 kg/m^3
EI	3.9150×10^{2} N·m^2
ζ_1	0.02
ζ_2	0.02
Central Body	
L_0 (radius)	2.0856 m
J_h	4.3497×10^{-2} kg·m^2

With the parameters defined, the stability of the rigid-flexible system can be studied by obtaining and analyzing the eigenvalues of the system. The eigenvalues of the system are listed in Table 5.2 for a system with a flexible structure divided into three elements of equal length for the FEM-based dynamics and six admissible functions for the ASM-based dynamics.

Table 5.2 Rigid-Flexible System Eigenvalues

FEM Eigenvalues (n=3)	ASM Eigenvalues ($\mathcal{A}$=6)
0	0
-19428.3	$-752.705 + j3375.68$
-4347.01	$-752.705 - j3375.68$
$-722.478 + j613.391$	$-338.670 + j2293.41$
$-722.478 - j613.391$	$-338.670 - j2293.41$
-728.760	$-123.158 + j1389.411$
-645.636	$-123.158 - j1389.411$
$-147.687 + j397.218$	$-33.2333 + j716.809$
$-147.687 - j397.218$	$-33.2333 - j716.809$
$-23.2402 + j153.182$	$-5.32560 + j266.226$
$-23.2402 - j153.182$	$-5.32560 - j266.226$
$-4.89025 + j32.2328$	$-1.03843 + j51.9113$
$-4.89025 - j32.2328$	$-1.03843 + j51.9113$
-8.08025	-1.73798

Based on the results displayed in Table 5.1, the rigid-flexible system for either formulated dynamics consists of a singule zero eigenvalue and several negative simple and complex conjugate eigenvalues for the rest. According to Lyapunov's indirect method summarized in Chapter 4, the rigid-flexible system is proven to be at least stable when under no control law.

When designing the full-state feedback control law and FO observer-based feedback control law, the system's output matrix is defined as $C = I_{2p}$. Creating the observability matrix with this output matrix shows that the system is completely observable because the observability matrix is found to be full rank. When designing the RO observer-based feedback control law, the system's output matrix becomes $C = [I_p \ \bar{0}_{p\times p}]$. Analysis of the observability matrix for this output matrix shows that it is also full rank, which means the system with the RO observer is also completely observable. The controllability matrix of the system does not show full rank. However, checking the rank of $[\lambda I - A \ B]$ for the only eigenvalue that is zero shows that the system is stabilizable, which is sufficient for the LQR control law.

5.1 Simulation Results

Several cases are simulated and studied to understand and analyze the characteristic behavior of the rigid-flexible structure with and without control laws. For all numerical simulations, the FEM-based dynamics are propagated following the explanation presented at the end of Chapter 3. The flexible structure is divided into 10 elements of equal lengths to ensure sufficiently accurate representation of flexible behavior while also considering necessary computational power.

5.1.1 Case A: No Control

For Case A, the rigid-flexible system is propagated over time without a control law. The flexible structure is given a nonzero initial translational and rotational nodal displacement that linearly increases as the nodes are located further away from the central rigid body.

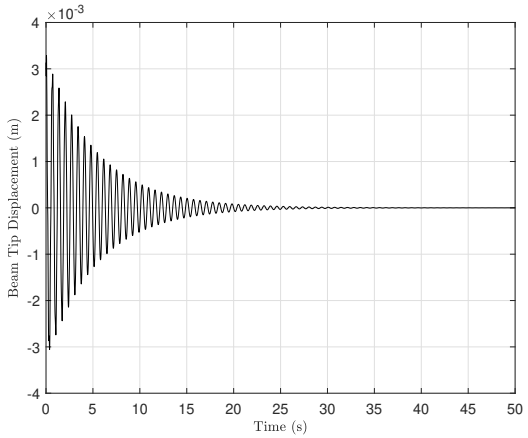

(a) Beam tip displacement relative to the body-fixed $\mathcal{B}$ frame

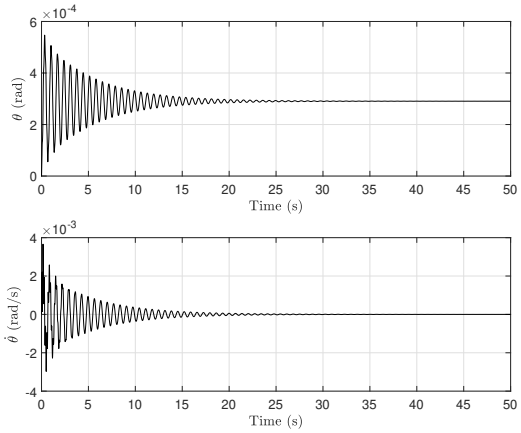

(b) Angular rotation θ and velocity $\dot{\theta}$ of the central rigid body

Figure 5.1 Translational and rotational motion of the flexible structure and central rigid body without control input.

When offset from its state of equilibrium, the flexible structure natural tends to return to stable equilibrium after several oscillations. The amplitude of oscillation, damping ratio, and settling time of the flexible structure are directly related to the physical properties of the flexible structure. Physical properties such as length, density, and flexural rigidity directly

impact the mass, damping, and stiffness matrices that describe the dynamic characteristics of the flexible structure. The damped oscillation of the flexible structure is visible in Figure 5.1(a). Furthermore, the motion of the flexible structure affects the motion of the rigid central body to which it is cantilevered. The rigid-flexible coupling between the flexible appendage and rigid central body is present in Figure 5.1(b) as the angular rotation and velocity of the central body also oscillate in a similar dampened fashion as the flexible structure, even settling at the same time. However, unlike the flexible structure, the central rigid body does not have a unique state of equilibrium. Although its angular velocity returns to zero, there is no stabilizing tendency that drives the central body back to its original angular position. Thus, the central body finds itself at rest in a different orientation, as shown in Figure 5.1(b).

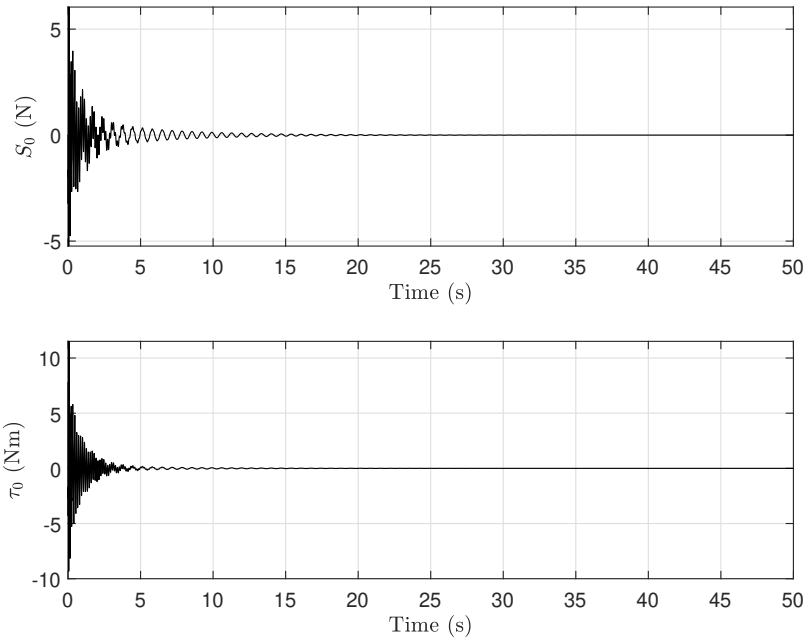

Figure 5.2 Shear force S_0 and bending moment τ_0 present at the root of the flexible structure without control input.

Figure 5.2 displays the shear force and bending moment, respectively, at the root of the flexible structure. Obtained from Eqs. (4.18) and (4.17), respectively, S_0 and τ_0 denote the

reaction force and moment due to the flexible structure. This is the rigid-flexible coupling present in the system. As the structure oscillates, so does the magnitudes of the shear force and bending moment, resulting in the oscillation of the central rigid body. A large shear force and bending moment magnitude is initially present due to the initial displacement of the flexible structure while the central body remains in the original position. These components decay towards zero as the flexible structure returns to a state of rest when no control is implemented. A central body with a larger moment of inertia will increase the settling time of the shear force and bending moment.

5.1.2 Case B: State-Feedback Control

For Case B, the full state-feedback control laws designed in Chapter 4 are applied to the rigid-flexible system. In each simulation, the system is given zero initial conditions, and a desired angular rotation $\theta_d = 5^\circ$ (0.0873 rad) and desired angular velocity $\dot{\theta} = 0$ rad/s for the central rigid body are specified. Table 5.3 presents the various control gains and parameters considered for the following full-state feedback simulations.

Table 5.3 Control Gains and Parameters for Full-State Feedback

Lyapunov-based Control	$a_1 = 100$, $a_2 = 300$, $a_3 = 99$, $a_4 = 500$	
LQR Control	$Q = \text{blkdiag}(\frac{1}{\theta_{max}^2}, \frac{1}{d_{y_{max}}^2}, \frac{1}{\phi_{max}^2}, \cdots, \frac{1}{\dot{\theta}_{max}^2}, \frac{1}{\dot{d}_{y_{max}}^2}, \frac{1}{\dot{\phi}_{max}^2}, \cdots)$ $\theta_{max} = 0.1$ rad, $d_{y_{max}} = 0.05$ m, $\phi_{max} = 0.05$ rad $\dot{\theta}_{max} = 0.1$ rad/s, $\dot{d}_{y_{max}} = 0.05$ m/s, $\dot{\phi}_{max} = 0.05$ rad/s $R = 5$ $C = I_{2p}$	
CSMC Control	$\text{sgn}(s)$ $\text{erf}(s)$ $\text{erf}(\frac{s}{\sqrt{2\sigma^2}})$	$C_{CSMC} = 10$ $K_{CSMC} = 0.001(\bar{1}_{1\times p})$ $\sigma = 0.1$
ASMC Control	$\varepsilon = 0.1$ $\eta = 0.001$ $\kappa_{g_0} = 0.005$ $\kappa_g(0) = 0.01$ $\Lambda = 10$ $\mu = 0.5$	

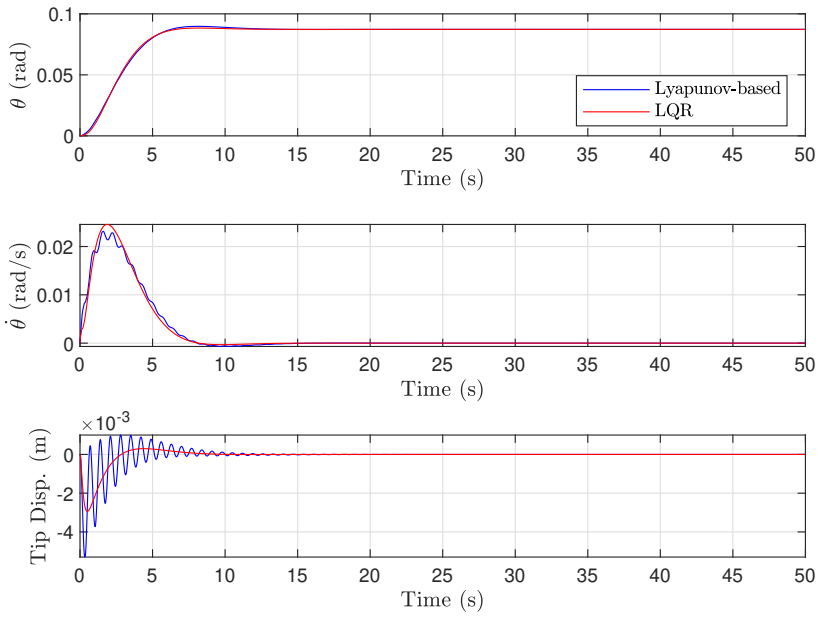

Figure 5.3 Angular rotation and velocity of the central rigid body and beam tip displacement of the flexible structure when applying full-state feedback.

A comparison of the results from implementation of the Lyapunov-based control law and the LQR in Figure 5.3 immediately depicts the difference in control behavior. While both full-state feedback control laws accomplish the control objectives, difference in vibration suppression during motion is notable. The Lyapunov-based control law invokes several vibrations present in the displacement of the beam, which in turn causes coupled oscillations in the angular rotation and, more noticeably, in the the angular velocity of the central rigid-body. The LQR control law produces a single offset in displacement of the flexible structure with some small overshoot before reducing it to zero again. Figure 5.4 displays the control input from both full-state feedback control laws. The LQR invokes a larger control input that changes rapidily at the beginning onto the system to satisfy the cost function demand on the system states that reduces flexible vibrations during motion. The Lyapunov-based control input is initially smaller, but quickly matches the input from the LQR with some oscillations due to the structural-flexible interaction with the control system.

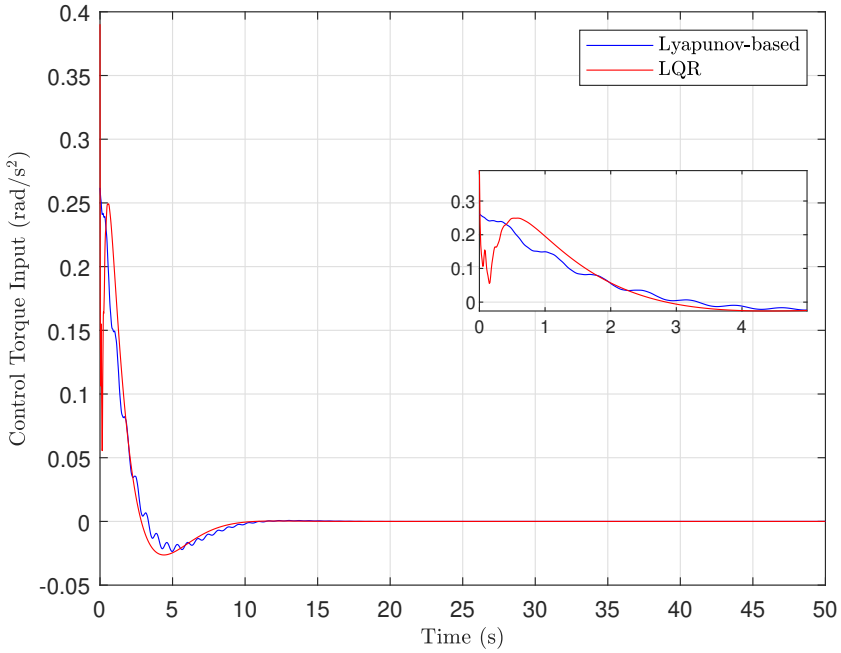

Figure 5.4 Control torque input for the Lyapunov-based control and LQR control.

Full-State Feedback Control Law with SMC

The previous simulations of the rigid-flexible system with the applied full-state feedback control laws assumed an ideal system without uncertainties. To incorporate model uncertainties in the simulations, the system equations of motion in Eq. (4.36) include a 20% uncertainty in the global mass, damping, and spring matrices. The model uncertainty is compensated by the inclusion of an SMC. The following numerical simulations present results of the additional control effort provided by the four different SMCs listed in Table 5.3.

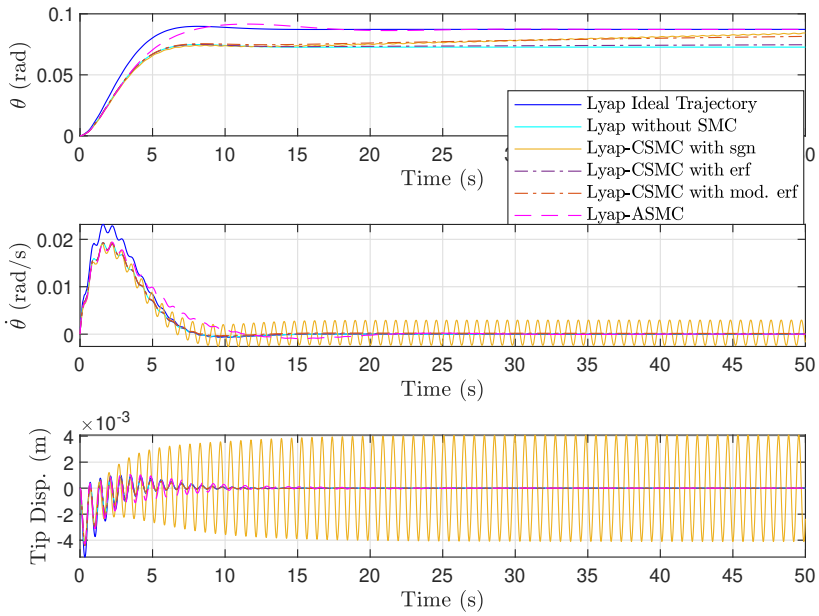

Figure 5.5 Angular rotation and velocity of the central rigid body and beam tip displacement of the flexible structure when applying the Lyapunov-based control with SMC.

Analysis of Figure 5.5 shows that the rigid-flexible system without the additional control effort from the SMC settles at a steady-state error from the desired θ_d. It requires a greater control input to move a system with an additional 20% mass. An increase in damping and stiffness also decreases the time of oscillation and increases the vibration frequency of the system, respectively. This makes controlling the system and achieving the control objectives more difficult. Applying the appropriate SMC with proper tuning can reduce the steady-state error caused by the uncertainties.

The CSMC with the sgn function reduced the steady-state error between the uncertain system and ideal system; however, the discontinuous nature of the sgnfunction that provides full control effort instantaneously at each time step, visible in Figure 5.6, results in significant chattering in the system. The only SMC that did not come close to reducing the steady-state error within the 50 s time span is the CSMC that utilizes the general error function $\text{erf}(s)$. While insufficient tuning of the parameters may be responsible for this result, another

probable cause that resulted in the CSMC to produce a small u_{SMC} input may be the very nature of the error function. By providing a smooth, continuous transition instead of an instantaneous but discontinuous transition, the control law may not have been able to apply to entire control effort in time before switching direction. In fact, this exact effect is demonstrated by the results from the CSMC with the modified error function $\text{erf}(\frac{s}{\sqrt{2\sigma^2}})$. By setting the standard deviation to $\sigma = 0.1$, the input in the error function is increased by a factor of 7.0711. This significant increase in value permitted the CSMC to apply more of the control effort to the system and reduce the steady state error in θ by more than half within the 50 s simulation time. The ASMC successfully reduced the steady-state error in a significantly shorter time span compared to CSMCs without any chattering. It is important to note that the oscillations present at the beginning of the simulation is not caused by chattering but by the vibrations of the flexible structure.

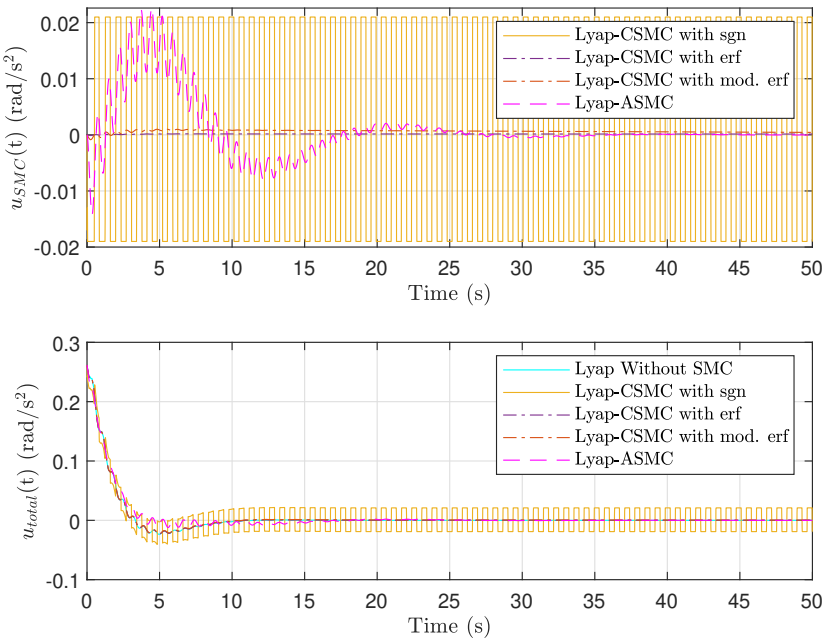

Figure 5.6 Control torque input from the SMC (top) and in combination with the Lyapunov-based control law (bottom).

The control inputs of each SMC are presented in Figure 5.6. As stated before because the

general error function does not allow enough time for the entire control effort to be applied, the control input from the CSMC with erf(s) is nonzero but small, which results in the long convergence time between the ideal trajectory and actual systems trajectory. The control input produced by the CSMS with the modified error function is slightly larger because the error function's input is increased by a factor of 7.0711, allowing more of the control effort to be applied before switching logic direction. The adaptive law in the ASMC that tunes the upper bounded gain in real-time allows for the proper amount of control effort to be applied over the entire simulation time span. Figure 5.7 displays the sliding manifold defined for each SMC with the Lyapunov-based control law and reinforces the analyzed behavior of the SMCs in Figures 5.5 and 5.6.

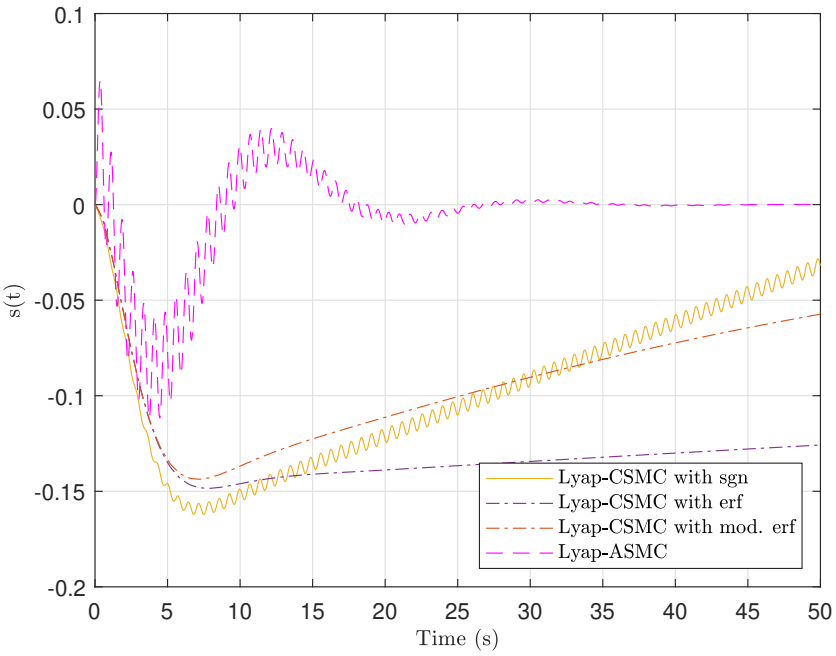

Figure 5.7 Sliding manifold for each SMC with the Lyapunov-based control law.

Figure 5.8 presents the simulated results of the a system with the same uncertainties; however, a full-state LQR feedback control is applied instead of the Lyapunov-based control law. According to the result shown in Figure 5.8, the CSMC with the sgn function reduces the steady-state error between the ideal system and the system with uncertainties; however,

chattering is, once again, prominent, significantly increasing the vibrational amplitude of the flexible structure. The CSMC with the general error function fails to provide a sufficient control effort to compensate for the uncertainties within the 50 s time span. The CSMC with the modified error function reduces the steady-state error by approximately half within the simulated time span without chattering, and the ASMC reduces the steady-state error within a quick convergence time while avoiding any chattering.

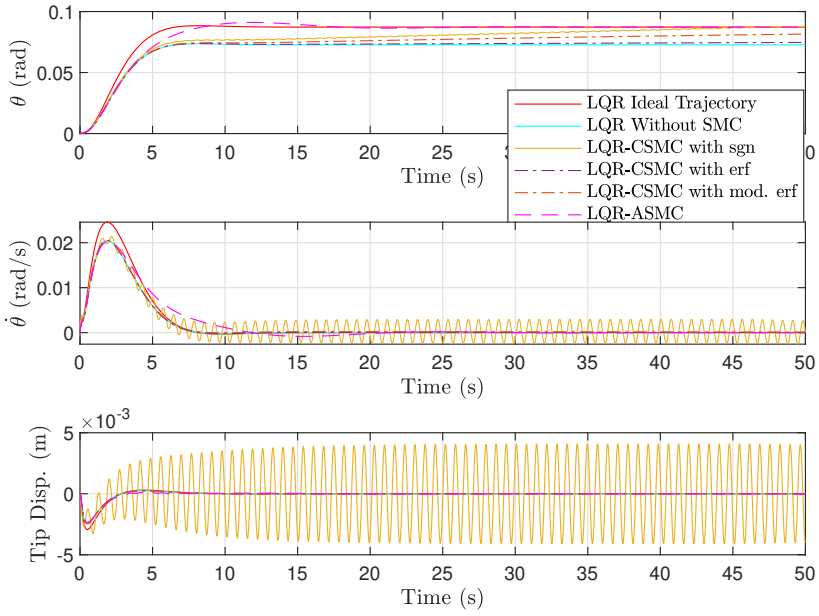

Figure 5.8 Angular rotation and velocity of the central rigid body and beam tip displacement of the flexible structure when applying the LQR control with SMC.

The resulting control inputs of the SMCs with the LQR control law resemble the control inputs with the Lyapunov-based control law but without the additional vibrations. The vibration suppression from the LQR control is shown to improve the performance of the SMCs. The convergence time between the ideal trajectory and actual system is slightly reduced for all three CSMCs, most notably the CSMC with sgn(s). The maximum control effort required from the ASMC is also slightly reduced. All of the trajectories on the sliding manifold in Figure 5.10 reflect the observed behavior and have either returned to $s = 0$ or

are returning to it.

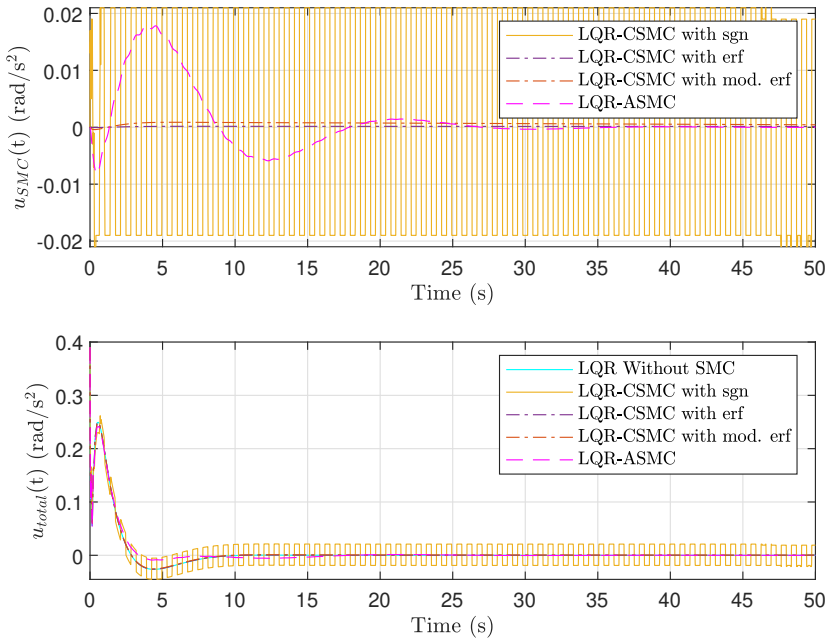

Figure 5.9 Control torque input from the SMC (top) and in combination with the LQR control law (bottom).

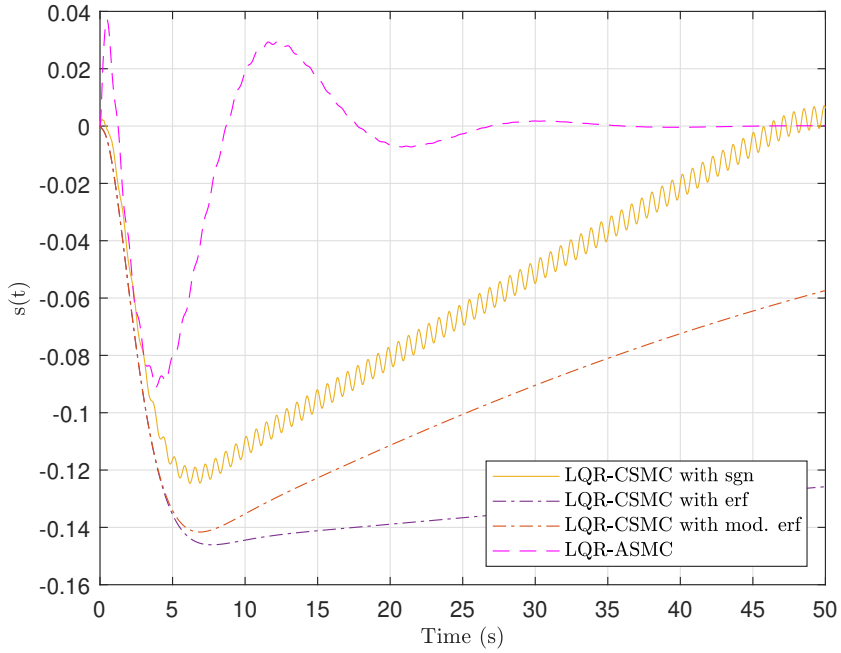

Figure 5.10 Sliding manifold for each SMC with the LQR control law.

5.1.3 Case C: Observer-based Feedback Control

For Case C, the full state-feedback control laws designed in Chapter 4 are no longer considered full-state. Instead, the FO and RO observers designed in Chapter 4 are implemented into the rigid-flexible system. In each simulation, the system is given zero initial conditions, and a desired angular rotation $\theta_d = 5^\circ$ (0.0873 rad) and desired angular velocity $\dot{\theta} = 0$ rad/s for the central rigid body are specified. The initial estimated states for the observers are provided by the MATLAB function `rand`, which returns uniformly distributed random numbers in the interval (0,1). The various control gains and parameters considered for the following observer-based feedback simulations are the same as the ones presented in Table 5.3 except for a one difference. The output matrix utilized in the reduce-order observer-based control simulations becomes $C = [I_p \ \bar{0}_{p\times p}]$.

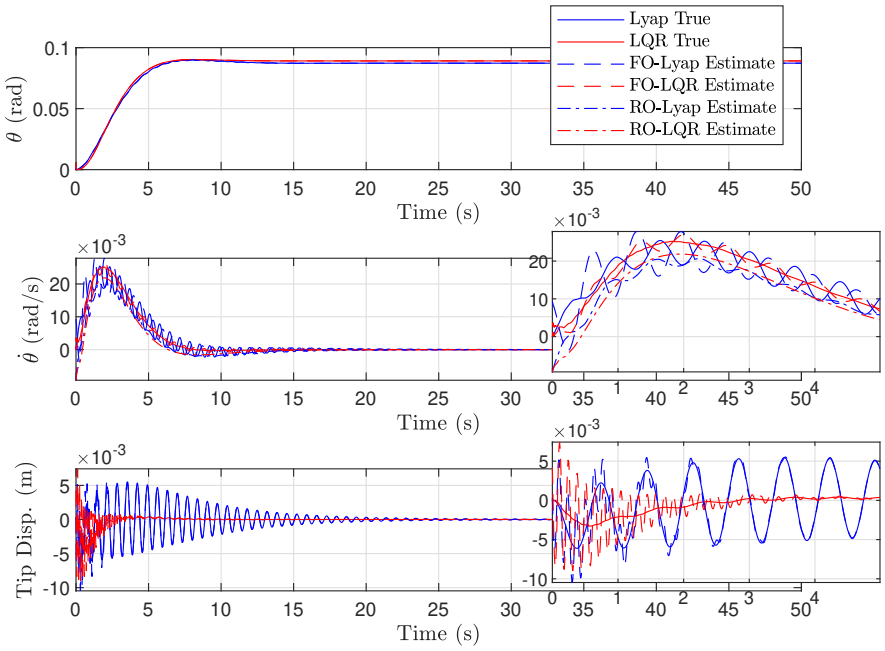

Figure 5.11 Angular rotation and velocity of the central rigid body and beam tip displacement of the flexible structure when applying a full-order and reduced-order observer-based controller with Lyapunov-based control and LQR control.

An important difference between the simulations in Case B and in Case C is the rigid-flexible system's measurement matrix. In an ideal case, all the states are assumed known and

measurable. However, in the real world, only the position states are generally measurable with sensors. Therefore, an observer is needed to estimate the unmeasurable states for feedback control. In Figure 5.11, the FO observer with brings the estimated angular rotation and tip displacement to the true states within less than 5 s. However, it takes more time to converge the estimated angular velocity with its true state for control laws. The FO estimated angular velocity shows excessive oscillating errors about the true angular velocity before converging after approximately 20 s. Implementation of the RO observer, however, reduces this oscillating error, replacing it with an offset error, and more closely matches the shape of the true state's trajectory as it converges within approximately 15 to 20 s. The control inputs computed from the FO and RO observer-based feedback controllers in Figure 5.12 show some deviation and oscillations within the first 5 s, but soon converge to match the full-state feedback control input.

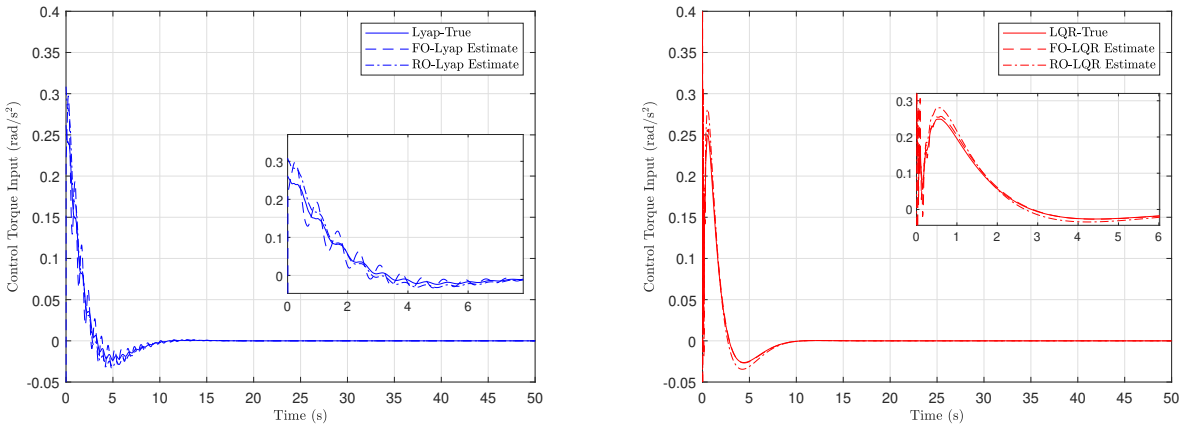

(a) Observer-based feedback control with Lyapunov-based control.

(b) Observer-based feedback control with LQR control.

Figure 5.12 Control torque input for the full-order and reduced-order observer-based controllers with Lyapunov-based control (a) and LQR control (b).

Observer-based Feedback Control Law with SMC

In a similar fashion to the numerical simulations in Case B, the rigid-flexible system is given the same model uncertainties. Because the actual system can only measure the position states, a FO observer-based feedback control and different SMCs are applied to the

system. Unlike the case with the full-state feedback control, the error dynamics between the ideal system and actual system used in the sliding manifold is a function of the ideal states and estimated actual states.

Figure 5.13 displays the propagated dynamics of system with FO observer-based feedback control and the different SMCs. Unlike the results for full state feedback, the CSMC with the sgn function produced an overshoot for θ and a large chattering at the beginning, more notably with the Lyapunov-based control than the LQR control. Furthermore, the convergence time has reduced significantly. However, the large chattering is not suitable for real-life application. The CSMC with the general error function continues to show low control effort with both the Lyapunov-based and LQR controls. The ASMC also continues to produce quick convergence with no chattering.

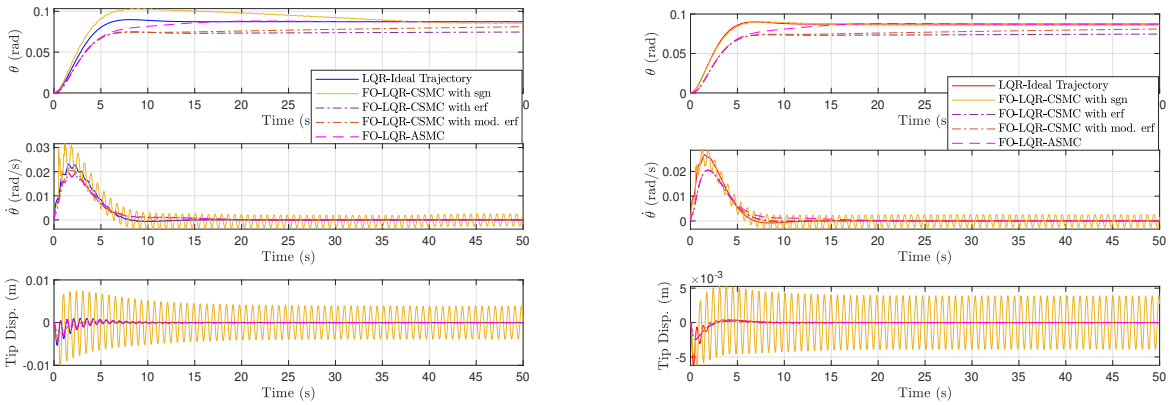

(a) Observer-based feedback control with Lyapunov-based control.

(b) Observer-based feedback control with LQR control.

Figure 5.13 Angular rotation and velocity of the central rigid body and beam tip displacement of the flexible structure when applying the full-order observer with Lyapunov-SMC control (a) and LQR-SMC control (b) .

The control inputs from the SMCs are shown in Figure 5.14. The large chattering from the CSMC with sgn(s) shows concentrated control effort near the maximum upper bound. With the implementation of the FO observer, the error function checks the difference between the ideal states and the actual estimated states. Because the observer is initially trying to

estimate the actual true states, the error function in the sliding manifold is larger, resulting in a larger control input from the CSMC. This, in turn, would explain the overshoot in θ, especially for the case with the Lyapunov-based control that does not suppress the vibration of the flexible structure as well as the LQR control. The other CSMCs produced similar control inputs as the full-state simulations since the control effort is limited. The ASMC produces a large initial control input as it is working with the estimated states, but it quickly diminishes within its upper bound. Figure 5.15 also displays the aggressive real-time tuning of the ASMC gain $K_{ASMC}(t)$ by the adaptive law at the very beginning as the ASMC works with the estimated states to return to the desired sliding manifold.

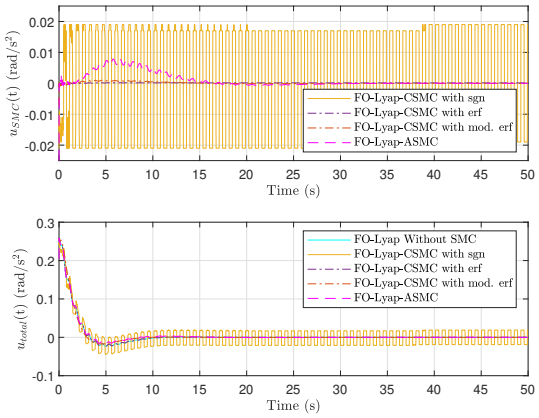

(a) Observer-based feedback control with Lyapunov-based control.

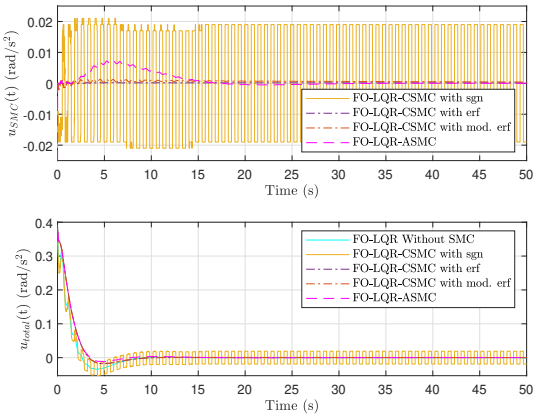

(b) Observer-based feedback control with LQR control.

Figure 5.14 Control torque input from the SMC (top) and in combination with the full-order observer-based feedback control (bottom).

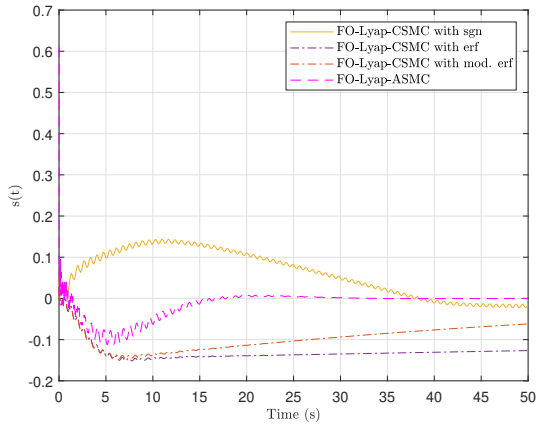

(a) Observer-based feedback control with Lyapunov-based control.

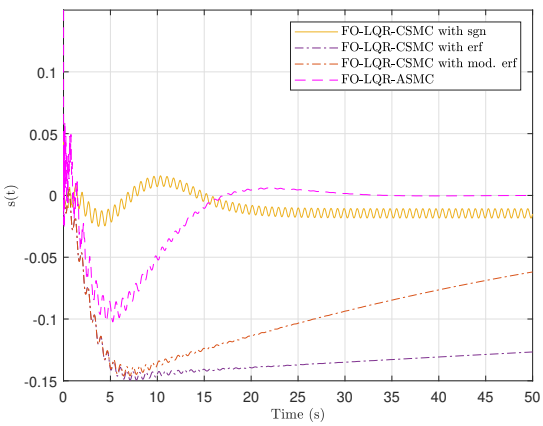

(b) Observer-based feedback control with LQR control.

Figure 5.15 Sliding manifold for each SMC with the full-order observer-based feedback control.

The final numerical simulations in Case C propagate the rigid-flexible system with uncertainties under the applied control of the RO observer-based feedback control with LQR and the different SMCs. Implementation of the RO observer to estimate only the unmeasurable velocity states proves to be more efficient than the FO observer. Because the error dynamics between the actual system with uncertainties and ideal system utilize the known position states and estimated velocity states, only the estimation error from the velocity states is present, reducing the difficulty for the SMCs. In fact, Figure 5.16 shows that the CSMC with sgn(s) no longer produces an overshoot with the Lyapunov-based control but, instead, more closely resembles the full-state simulation. The tip displacement of the flexible structure also no longer has a large chattering at the very beginning for either the Lyapunov-based control and LQR control. Once again, the other SMCs produced similar results as the full-state simulations.

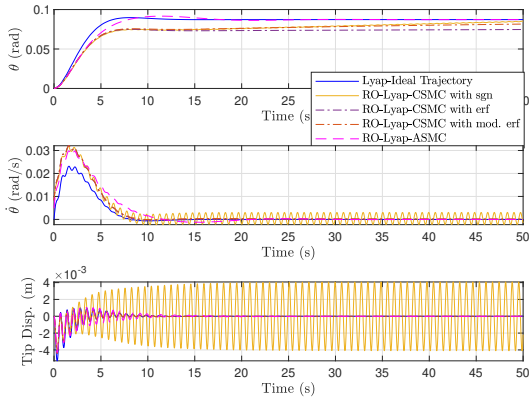

(a) Observer-based feedback control with Lyapunov-based control.

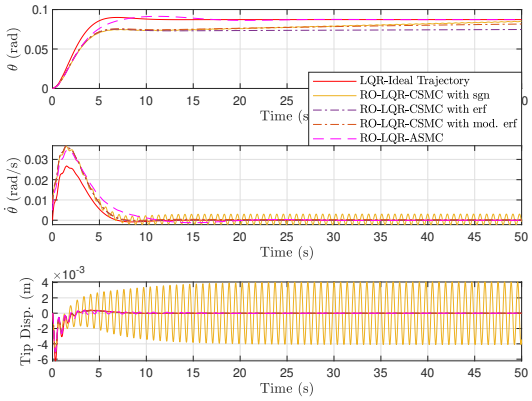

(b) Observer-based feedback control with LQR control.

Figure 5.16 Angular rotation and velocity of the central rigid body and beam tip displacement of the flexible structure when applying the reduced-order observer with Lyapunov-SMC control (a) and LQR-SMC control (b) .

However, the control input from these other SMCs is significantly smaller when the RO observer is implemented. In Figure 5.16, the control input for the ASMC is on the scale of 10^{-3} with both the Lyapunov-based and LQR control laws. The overall deviation from the desired sliding manifold is also significantly smaller for the case with a reduce-order observer, as shown in Figure 5.18.

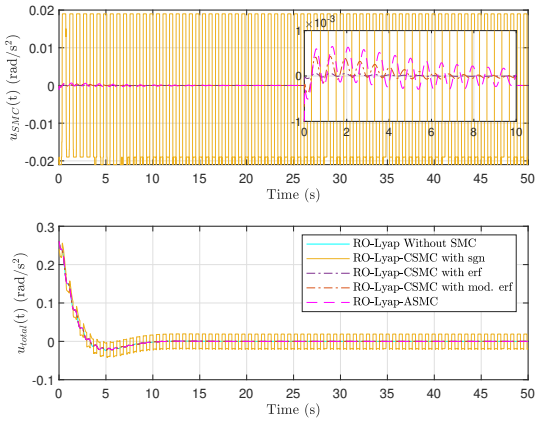

(a) Observer-based feedback control with Lyapunov-based control.

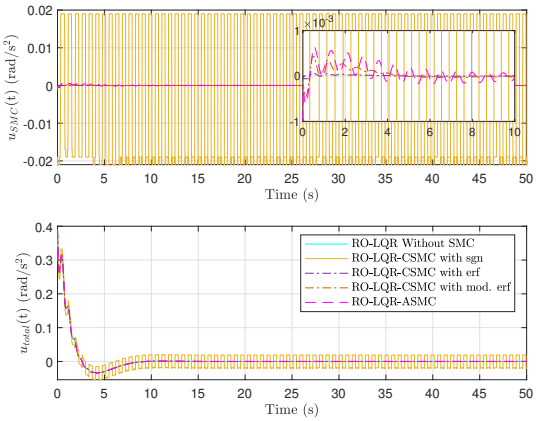

(b) Observer-based feedback control with LQR control.

Figure 5.17 Control torque input from the SMC (top) and in combination with the reduced-order observer-based feedback control (bottom).

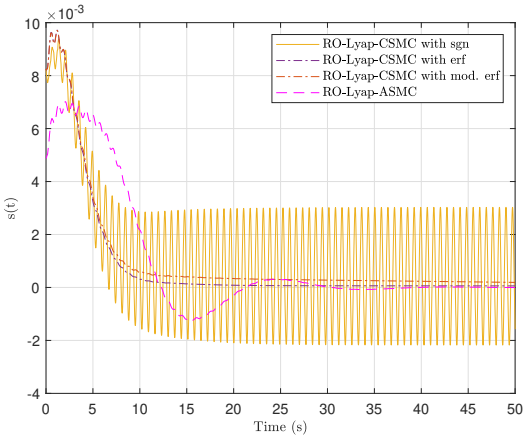

(a) Observer-based feedback control with Lyapunov-based control

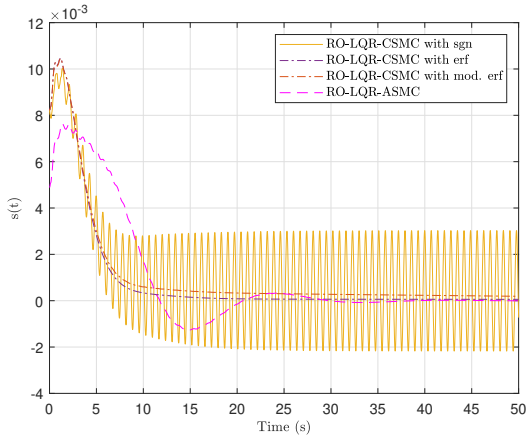

(b) Observer-based feedback control with LQR control.

Figure 5.18 Sliding manifold for each SMC with the reduced-order observer-based feedback control.

6 Conclusion and Future Work

This chapter presents the concluding remarks that summarize the results obtained using the methods described in this thesis to formulate the dynamics of a space vehicle with a flexible structure and the designed control laws that stabilize and control the rigid-flexible system. Potential ideas of future research and current research for this work following this thesis are also presented.

6.1 Conclusion

In this thesis, the dynamics of a space vehicle with a flexible structure has been formulated and studied, and full-state and observer-based feedback control systems have been designed and analyzed for the rigid-flexible system. The nonlinear ordinary and partial differential equations of motion of a rigid-flexible system have been linearized through the application of two different discretization techniques: the assumed modes method (ASM) and the finite element method (FEM). The discretization of the system's dynamics in conjunction with the Lagrangian equations yielded a system of undamped vector-matrix second-order differential equations that also included the rigid-flexible coupling present in such as system. Damping was included in the form of proportional damping to increase the accuracy of the modeled equations of motion. The dynamics formulated by through FEM were selected for control design and numerical simulation for several reasons. FEM utilizes general coordinates that directly reflect the physical behavior and motion of the system. In order to calculate the displacement of a point along the flexible structure, a series summation of all the admissible functions at that location is required. This makes it very ineffective in application with control laws that require multiple positions along the flexible structure. FEM also provides greater versatility than ASM, which allows for easier modification of the system model for any future research.

Analysis of the system's stability through the application of Lyapunov's indirect method showed that the open-loop rigid-flexible system is at least neutrally stable with all real, distinct negative eigenvalues and one zero eigenvalue. Lyapunov's direct method was also

applied. Using an energy-based Lyapunov candidate function, the closed-loop rigid-flexible system was proven to be asymptotically stable with the presented Lyapunov-based control law. Observability and controllability analysis of the system showed that the system is fully observable and at least stabilizable.

The control laws designed for the rigid-flexible system presented and studied are closed-loop feedback control laws that utilize the feedback of the system's states to apply corrective control input to achieve the desired system orientation while suppressing the vibrations of the flexible structure. Along with the Lyapunov-based control law, a linear quadratic regular (LQR) was designed by minimizing the quadratic cost function and computing the control gain by solving for the algebraic Riccati equation. Although the formulated dynamics provide an accurate approximation of the true system dynamics, uncertainties in the model are unavoidable. To correct for these uncertainties, sliding mode control (SMC) laws are presented for their robustness in accommodating for uncertainties and disturbances. The conventional SMC (CSMC) with a linear sliding manifold is studied with several variation in the CSMC control law. To mitigate the chattering often present in CSMCs, the sgn function is replaced with the general error function and a modified error function. An adaptive SMC (ASMC) is also considered and presented. The ASMC utilizes a nonlinear sliding manifold and an adaptive law that tunes the upper bound SMC gain in real-time, attenuating chattering and eliminating the reaching phase. In extending this control to real-world application, a full-order (FO) observer and reduced-order (RO) observer are also designed and implemented in the feedback control system.

The rigid-flexible coupling is shown to effect the overall dynamics of the system. Without control, initial offset displacement or excitation of the flexible structure produces a reaction shear force and bending moment on the central rigid body at the root of the structure, affecting the motion of the central rigid body and resulting in a change in the system's orientation. In full-state feedback of an ideal rigid-flexible system, both the Lyapunov-based control and LQR control reached the desired angular rotation θ of the central rigid body

within the same settling time. The LQR control demanded a larger and greatly varying initial control input, but the Lyapunov-based control did not suppress the vibration of the flexible structure as effectively during motion.

It is shown that inclusion of uncertainty in the system model produces a steady-state error in θ. The simulated results for full-state feedback with both the Lyapunov-based control and LQR control showed that the CSMCs either produced significant chattering or required a greater factor in the error function to converge the actual system with uncertainties to the ideal trajectory within the 50 s time span. The ASMC, however, consistently reached the ideal trajectory with a very small convergence time and without demanding a relatively large amount of control input. When the FO observer was implemented, the initial error in state estimation due to the unsuppressed vibrations from the Lyapunov-based control showed to introduce excessive control input for the CSMC with $\text{sgn}(s)$, resulting in an overshoot much greater than that produced for the system with the LQR control. The RO observer did not produce this effect since the observer is only estimated the velocity states. Instead, implementation of the true position states and estimated velocity states yielded a smaller and more oscillating control effort by the SMCs, especially the ASMC.

6.2 Future Work

This research provided a reliable framework of dynamics and control that can be conveniently extended to different rigid-flexible system models and control designs. Some future and current work based on the current study are summarized below.

The flexible structure in this work was assumed as an Euler-Bernoulli beam since it can represent the characteristics of the flexible beam with sufficient accuracy. However, the necessary assumptions associated with the Euler-Bernoulli beam limits the model accuracy, especially for three-dimensional motion. A possible alternative would be the Timoshenko beam. The Timoshenko beam includes the idea of shear deformation that is present when a beam deforms, improving the model accuracy. The Timoshenko beam has been the subject of significant research in the field of aerospace engineering and structural dynamics and

has already been applied to the rigid-flexible spacecraft system. However, to the author's knowledge, not as much control law design has been implemented for the Timoshenko beam as it has for the Euler-Bernoulli beam.

Experimental implementation of designed control laws can also be considered as future work. It is important to ensure that theoretical control laws effectively work in real-life applications that introduce discrete systems and limited sensors. The author is currently working on a project that studies flexible body control using fiber optic strain sensors (FlexFOS). The research examines the feasibility and efficacy of fiber optic strain sensors as a means of obtaining dynamic measurement data of a flexible structure that can be used to control the rigid-flexible system. Properly modeled dynamics of a rigid-flexible system and observer-based feedback control laws are integral in the experimentation of FlexFOS.

The author also has prior experience in studying rigid-body spacecraft with onboard robotic manipulators. Similar in idea to FEM, several outside works have considered treating flexible structures as a combination of several rigid-body linked robotic manipulators in which the flexible nature of a flexible structure is incorporated in the hinges between each link. However, flexible manipulators have also become a subject of great interest over recent years, especially with rising interest in on-orbit servicing and manufacturing and space debris collection. All of the aforementioned systems involve nonlinear coupled dynamics between a central rigid body or hub and some protruding and less rigid, or even flexible, appendage.

ACKNOWLEDGMENT OF FUNDING

Support from the Department of Education Graduate Assistance in Areas of National Need (GAANN) and the Deep Space Logistics Office at NASA Kennedy Space Center (Contract No. AIS-E3-21-002) is gratefully acknowledged.

REFERENCES

[1] Logan, D. L., *A First Course in the Finite Element Method*, 4th ed., Thomson Canada Limited, 2007.

[2] Waymeyer, W. K., and Sporing, R. W., "An Industry Survey on Aeroelastic Control System Instabilities in Aerospace Vehicles," *IAS 30th Annual Meeting)*, New york City, New York, 1962.

[3] Deyst, J., "A survey of structural flexibility effects on spacecraft control systems," *7th Aerospace Sciences Meeting*, New York City, NY, 1969. https://doi.org/10.2514/6.1969-116.

[4] "Effects of Structural Flexibility on Spacecraft Control Systems," 1969.

[5] Likins, P. W., *Dynamics and control of flexible space vehicles*, Legacy CDMS, 1970.

[6] Hooker, W. W., and Margulies, G., "The Dynamical Attitude Equations for an n-Body Satellite," *Journal of the Astronautical Sciences*, Vol. 12, 1965, pp. 123–128.

[7] Roberson, R. E., and Wittenberg, J., "A Dynamical Formalism for an Arbitrary Number of Interconnected Rigid Bodies, with Reference to the Problem of Satellite Attitude Control," *Proceedings of the Third International Congress of Automatic Control (London, 1966)*, Butterworth & Co., Ltd., London, England, 1967.

[8] Farrell, J. L., Netwon, J. K., and Connelly, J. J., *Digital program for dynamics of non-rigid gravity gradient satellites*, National Aeronautics and Space Administration, 1968, Washington, D. C., 1968.

[9] Fleischer, G. E., *Multi-rigid body attitude dynamics simulation*, Pasadena, California, 1971.

[10] Russell, W. J., *ON THE FORMULATION OF EQUATIONS OF ROTATIONAL MOTION FOR AN N-BODY SPACECRAFT*, 1969.

[11] Spencer, T. M., "A Digital Computer Simulation of the Attitude Dynamics of a Spin-Stabilized Spacecraft," *AAS Symposium on Rocky Mountain Resources for Aerospace Science and Technology*, Butterworth & Co., Ltd., 1967.

[12] Meirovitch, L., *Fundamentals of Vibrations*, McGraw-Hill, 2001.

[13] Meirovitch, L., *Analytical Methods in Vibrations*, Macmillan Company, Toronto, Canada, 1967.

[14] Meirovitch, L., *Principles and Techniques of Vibrations*, Prentice-Hall, Inc., 1997.

[15] Zhou, S.-T., Chiu, Y.-J., Guo-Fei, Y., Chia-Hao, Y., Hong-Wu, H., and Sheng-Rui, J., "An assumed mode method and finite element method investigation of the coupled vibration in a flexible-disk rotor system with lacing wires," *Journal of Mechanical Science and Technology*, Vol. 31, No. 2, 2017, pp. 577–586.

[16] Theodore, R., and Ghosal, A., "Comparison of the Assumed Modes and Finite Element Models for Flexible Multilink Manipulators," *I. J. Robotic Res.*, Vol. 14, 1995, pp. 91–111. https://doi.org/10.1177/027836499501400201.

[17] Wang, Y., and Huston, R., "A lumped parameter method in the nonlinear analysis of flexible multibody systems," *Computers & Structures*, Vol. 50, No. 3, 1994, pp. 421–432.

[18] Chen, L., and Deng, H., ""Model reduction of rigid-flexible manipulators with experimental validation," *Advanced Materials Research*, Vol. 655-657, No. 1, 1994, pp. 1101–1107.

[19] Vakil, M., Fotouhi, R., and Nikiforuk, P., "Trajectory Tracking for the End-effector of a Class of Flexible Link Manipulators," *Journal of Vibration and Control*, Vol. 17, No. 1, 2011, pp. 55–68.

[20] Pepper, D. W., *The Finite Element Method: Basic Concepts and Applications with*

MATLAB, MAPLE, and COMSOL, 3rd ed., Series in computational and physical processes in mechanics and thermal sciences, CRC Press, Boca Raton, FL, 2017.

[21] Dwivedy, S. K., and Eberhard, P., "Dynamic analysis of flexible manipulators, a literature review," *Mechanism and Machine Theory*, Vol. 41, No. 7, 2006, pp. 749–777. https://doi.org/https://doi.org/10.1016/j.mechmachtheory.2006.01.014.

[22] Jiang, H., van der Veek, B., Kirk, D., and Gutierrez, H., "Real-Time Estimation of Time-Varying Bending Modes Using Fiber Bragg Grating Sensor Arrays," *AIAA Journal*, Vol. 51, No. 1, 2013, pp. 178–185. https://doi.org/10.2514/1.J051702.

[23] Kiang, C. T., Spowage, A., and Yoong, C. K., "Review of Control and Sensor System of Flexible Manipulator," *Journal of Intelligent & Robotic Systems*, Vol. 77, No. 1, 2015, pp. 187–213.

[24] Palomba, I., Richiedei, D., and Trevisani, A., "Reduced-Order Observers for Nonlinear State Estimation in Flexible Multibody Systems," *Shock and Vibration*, Vol. 2018, 2018, pp. 1–12.

[25] Lu, L., Chen, Z., Yao, B., and Wang, Q., "A Two-Loop Performance-Oriented Tip-Tracking Control of a Linear-Motor-Driven Flexible Beam System With Experiments," *IEEE Transactions on Industrial Electronics (1982)*, Vol. 60, No. 3, 2013, pp. 1011–1022.

[26] Krstic, M., Guo, B.-Z., Balogh, A., and Smyshlyaev, A., "Control of a Tip-Force Destabilized Shear Beam by Observer-Based Boundary Feedback," *SIAM Journal on Control and Optimization*, Vol. 47, No. 2, 2008, pp. 553–574.

[27] Yan, R., and Wu, Z., "Attitude stabilization of flexible spacecrafts via extended disturbance observer based controller," *Acta Astronautica*, Vol. 133, 2017, pp. 73–80.

[28] Dogan, K. M., Gruenwald, B. C., Yucelen, T., and Muse, J. A., "Adaptive architectures for control of uncertain dynamical systems with actuator and unmodeled dynamics," *International Journal of Robust and Nonlinear Control*, Vol. 29, No. 12, 2019, pp. 4228–4249. https://doi.org/https://doi-org.ezproxy.libproxy.db.erau.edu/10.1002/rnc.4624.

[29] Gaudiller, L., and Bochard, S., "Adaptive active control of flexible structures subjected to rigid body displacements," *Journal of Sound and Vibration*, Vol. 283, No. 1, 2005, pp. 311–339. https://doi.org/https://doi.org/10.1016/j.jsv.2004.04.039.

[30] Balas, M. J., and Frost, S. A., "Adaptive control of flexible structures using Residual Mode Filters," *49th IEEE Conference on Decision and Control (CDC)*, 2010, pp. 2620–2624. https://doi.org/10.1109/CDC.2010.5717064.

[31] Cho, H., Kerschen, G., and Oliveira, T. R., "Adaptive smooth control for nonlinear uncertain systems," *Nonlinear dynamics*, Vol. 99, No. 4, 2020, pp. 2819–2833.

[32] Gere, J. M., *Mechanics of Materials*, 5$^{\text{th}}$ ed., Brooks/Cole Publishers, Pacific Grove, CA, 2001.

[33] Junkins, J. L., and Kim, Y., *Introduction to Dynamics and Control of Flexible Structures*, AIAA Education Series, American Institute of Aeronautics and Astronautics, Washington, DC, 1993.

[34] Fujii, H., Ohtsuka, T., and Udou, S., "Mission Function Control for Slew Maneuver Experiment," *Journal of Guidance, Control, and Dynamics*, Vol. 14, No. 06, 1991, pp. 986–992.

[35] Bisplinghoff, R. L., Ashley, H., and Halfman, R. L., *Aeroelasticity*, Addison-Wesley, Reading, MA, 1957.

[36] Meirovitch, L., *Elements of Vibration Analysis*, 2$^{\text{nd}}$ ed., McGraw-Hill Book Company, New York, NY, 1986.

[37] Meirovitch, L., *Dynamics and Control of Structures*, John Wiley & Sons, New York, NY, 1990.

[38] Junkins, J., and Turner, J., *Optimal Spacecraft Rotational Maneuvers*, North Holland, 1986.

[39] Craig, R. J., *Structural Dynamics - an Introduction to Computer Methods*, John Wiley & Sons, New York, NY, 1981.

[40] Brogan, W. L., *Modern Control Theory*, 3rd ed., Prentice Hall, Englewood Cliffs, N.J, 1991.

[41] Zhou, K., and Doyle, J. C., *Essential of Robust Control*, 1st ed., Prentice Hall, 1997.

[42] Fulton, J. M., "LQG/LTR Optimal Attitude Control of Small Flexible Spacecraft Using Free-Free Boundary Conditions," Ph.D. thesis, University of Colorado, 2006.

[43] Khalil, H. K., *Nonlinear Systems*, 3rd ed., Prentice Hall, 2001.

[44] Ordaz, P., Ordaz, M., Cuvas, C., and Santos, O., "Reduction of matched and unmatched uncertainties for a class of nonlinear perturbed systems via robust control," *International Journal of Robust and Nonlinear Control*, Vol. 29, No. 8, 2019, pp. 2510–2524. https://doi.org/https://doi-org.ezproxy.libproxy.db.erau.edu/10.1002/rnc.4506.

[45] Bracewell, R. N., *The Fourier Transform & Its Applications*, 3rd ed., McGraw-Hill, 2000.

[46] Andrews, L. C., *Special functions of mathematics for engineers*, 2nd ed., SPIE Press Monograph, SPIE Optical Engineering Press, Bellingham, Wash, 1997.

[47] McCann, B. S., Nazari, M., and Udwadia, F., "Analysis of Inequality Constraints without Using Lagrange Multipliers with Applications to Classical Dynamical Systems," *ASME 2022 International Mechanical Engineering Congress and Exposition IMECE 2022*, Columbus, OH, 2022.